FINAL REPORT

REVERSE MICELLE BASED SYNTHESIS OF MICROPOROUS MATERIALS IN MICROGRAVITY

(Supported by NASA Grant/Contract No. NAG3-1416)

Prof. Prabir K. Dutta
Department of Chemistry
The Ohio State University
120 West 18th Ave.
Columbus, OH 43210-1173
614 292 4532
Dutta.1@osu.edu

Executive Summary

Microporous materials play a very important role in chemical, petrochemical and environmental industries. The intracrystalline space in these materials consists of channels and/or cages of molecular dimensions, and is the site for much of the interesting chemistry. There is considerable effort worldwide in synthesis of frameworks with new topologies and frameworks. Complexity of the physical and chemical processes that occur during the hydrothermal synthesis of such materials has minimized progress in understanding the molecular events that are responsible for formation of specific frameworks. Yet, it is clear that the goal of tailor-directed synthesis rather than the current trial and error efforts will only become reality with a better understanding of the crystal growth process. Such is the objective of this research program.

The development of new methods for nucleating and growing microporous crystals has not only made available new structures and morphologies, but also provided insight into crystal growth. As part of the NASA-funded program, we reported in 1995 (*Nature*, volume 374, page 44) a new method for synthesis of zincophosphate with the sodalite structure. The crystals were made from reactants included within the microscopic aqueous droplets of reverse micelles dispersed in an organic solvent. Two inorganic components, zinc and phosphate ions are introduced in separate micelles and crystallization is dependent on the collision and exchange kinetics of the surfactant structures. Further studies have indicated that the rates of crystal growth can also be varied over a wide range by manipulating the intramicellar concentrations. Three growth processes, all resulting in sodalite formation have been discovered. These include a layer-by-layer growth by deposition of micellar contents on specific crystal faces, rapid agglomeration of nuclei of ~75 nm to form crystals and formation of crystal via reconstruction of an amorphous intermediate phase. ^{31}P NMR studies show that the intramicellar acidity is different in these three pathways. We have proposed that the different acidities result in different phosphate species and thereby supersaturation conditions for zincophosphate formation. For the case of lowest supersaturation, few nuclei are formed in the micelles and crystal growth needs to occur by acceptance of solution species in other micelles. This is a slow process, resulting in single crystals of well defined morphology. In the case of highest supersaturation, growth is rapid and since time for nucleation is limited, it results in amorphous particles. The third pathway, in which nuclei are found to aggregate represents an intermediate case.

The observation of distinct crystal growth pathways via the reverse micellar procedure provides an excellent opportunity to study these in detail. Presently, the growth processes are all interrupted by sedimentation when particles reach size of half a micron. In microgravity, the growth process is expected to continue. It has been reported that particles in a fluid which will sediment due to gravitational forces can be kept suspended by rotation of the reaction chamber. We have constructed a rotating cell and examined all three pathways with it. Indeed, crystal growth could be accomplished without sedimentation. However, further information on crystal growth could not be obtained in all cases. It appears that rotation has two effects. First, it promotes crystal aggregation, presumably from increased collisions of particles with each other. Second, the rapid motion of nutrients around the crystals alters the crystal face development. Thus, it is expected that the absence of buoyancy driven convection in microgravity should allow us to examine the development of different crystal faces.

Abstract

Formation of zincophosphates from zinc and phosphate containing reverse micelles (water droplets in hexane) has been examined. The frameworks formed resemble that made by conventional hydrothermal synthesis. Dynamics of crystal growth are however quite different, and form the main focus of this study. In particular, the formation of zincophosphate with the sodalite framework was examined in detail. The intramicellar pH was found to have a strong influence on crystal growth. Crystals with a cubic morphology were formed directly from the micelles, without an apparent intermediate amorphous phase over a period of four days by a layer-by-layer growth at the intramicellar pH of 7.6. At a pH of 6.8, an amorphous precipitate rapidly sediments in hours. Sodalite was eventually formed from this settled phase via surface diffusion and reconstruction within four days. With a rotating cell, it was possible to minimize sedimentation and crystals were found to grow epitaxially from the spherical, amorphous particles. Intermediate pH's of 7.2 led to formation of aggregated sodalite crystals prior to settling, again without any indication of an intermediate amorphous phase. These diverse pathways were possible due to changes in intramicellar supersaturation conditions by minor changes in pH. In contrast, conventional syntheses in this pH range all proceeded by similar crystallization pathways through an amorphous gel. This study establishes that synthesis of microporous frameworks is not only possible in reverse micellar systems, but they also allow examination of possible crystallization pathways.

Introduction

Microporous materials include a large group of solids of varying chemical composition as well as porosity. The framework structure is made up of interconnecting T-O-T' bonds, where T and T' can be Si, Al, P, Ga, Fe, Co, Zn, B and a host of other elements.[1] Materials with Si-O-Al bonding in the framework are called zeolites and find extensive use.[2] Their microporous nature is exploited in a variety of adsorption and separation phenomena.[3] Ion-exchange properties of these materials are exploited in the consumer and environmental industries.[4] Chemical and petroleum industries use these materials as catalysts in hydrocarbon transformations.[5] Synthesis of new frameworks has led to new technologies, and considerable effort is being expended in their discovery.[3]

Microporous materials are typically synthesized by a hydrothermal process. Study of the nucleation, crystal growth as well as development of new synthesis conditions is an active area of research.[6] Crystal growth of these materials is a complicated chemical process.[7] For example, in zeolite formation, the silicon and aluminum containing reactants dissolve in the presence of base to produce soluble species. Speciation is strongly influenced by the pH, temperature, cations and structure directing agents. Insoluble aluminosilicates are rapidly formed by reaction of the solubilized species. Thus, this system is typically in a state of supersaturation for many of the aluminosilicate species. After an induction period that can extend from hours to weeks, crystals are observed in the system. Nuclei formation can occur by

solid state restructuring of the gel or precipitation from the supersaturated solution. The nuclei can grow using nutrients from the solution or the gel to form the crystals. The resulting crystal morphologies are controlled by preferential growth of crystal faces.

Our group has been interested in understanding the mechanism of zeolite crystal growth and have exploited Raman spectroscopy to investigate solution species, structure of the gel and template molecules during zeolite synthesis.[8] Considerable work has also been done using NMR spectroscopy to monitor solution species and derive information about the nucleation process.[9] Other techniques that have provided information on the early stages of zeolite nucleation include neutron scattering.[10] Though considerable research has been done on analysis of the structural aspects of species responsible for zeolite nucleation, much less is known about crystal growth. This issue is critical for several reasons. The competitive growth of nuclei into crystals determines the final crystalline product. Even though nuclei of a certain zeolitic framework may be formed readily, the rate of crystal growth may be limiting. Growth of large crystals and seeding phenomena are also dependent on the type of crystal growth. Finally, the morphology will depend on the crystal growth process.

Crystallization, in general, has been extensively studied over many decades.[11,13] Supersaturation of nucleating species has shown to profoundly affect the crystallization process. Walton has summarized the effects of initial supersaturation on crystal morphology.[12] It was noted that the morphology will vary from compact well

defined crystals to poorly developed crystals and finally amorphous aggregates as the initial supersaturation changes.[12] Examples are $ZnC_2O_4 \cdot 2H_2O$ whose crystals have different habits in different supersaturation ranges.[14] In the case of $CaHPO_4$, with increasing supersaturation, rhombohedral, intergrown and twinned crystals of $CaHPO_4 \cdot 2H_2O$ and ultimately, spherical agglomerates of $CaHPO_4$ are formed.[15]

To the best of our knowledge, the influence of supersaturation on growth of microporous frameworks has not been systematically examined. We report here the discovery that by using reverse micelles as reactants for the growth of zincophosphate sodalite framework, control can be exercised over the supersaturation levels, and distinct crystal growth pathways are observed.

Certain surfactant molecules, dissolved in organic solvents, are capable of solubilizing water in the polar core and these entities are called reverse micelles or microemulsions. Reverse micelles have the ability to solubilize macromolecules and enzymes and enzymatic chemistry in these systems is dependent on the water content of the micelles.[16] Polymerization chemistry is also possible in reverse micelles, including control of gel formation and/or flocculation.[17] There has also been considerable work on controlled synthesis of inorganic particles using reverse micelles, including those of semiconductors, metals, oxides and carbonates.[18] The dynamic behavior of reverse micelles, i.e. the fact that the species in different micelles can interact with each other via collisions is important in the particle nucleation and growth process. A connection between the micellar environment and the final morphology of the material, including the state of aggregation has been found to

exist.[17]

These studies motivated us to explore if reverse micelles can be used to form microporous materials. Our attempts to grow aluminosilicate zeolites at >60°C were unsuccessful because of instability of reverse micelles at high temperatures.[19a] Intermicellar attractive forces increase upon raising the temperature, resulting in phase separation.[20] Thus, in order to study the crystal growth characteristics of microporous materials in reverse micelles, we had to limit ourselves to frameworks that can be made under ambient conditions. Stucky and coworkers have recently shown that zincophosphate microporous materials, with frameworks similar to that of the aluminosilicate zeolites can be synthesized under ambient conditions.[21] We have shown in an earlier communication that zinc and phosphate ions introduced via reverse micelles will interact with each other and lead to the nucleation and subsequent growth of zincophosphate sodalite crystals.[19b] In this study, we explore this system in more detail. The particle size development, their crystallinity and morphology during crystal growth process has been studied. We demonstrate here that by controlling the internal pH of these assemblies, and thereby supersaturation, important information about the crystal growth process is obtained.

Experimental Section

Materials: The surfactant sodium bis (2-ethyl hexyl) sulfosuccinate (AOT) (Aldrich,

> 98%), n-hexane (Fisher, 99.9%), zinc nitrate hexahydrate (Aldrich, 98%), H_3PO_4 (AR Grade, Mallinckrodt, 85%), tetramethylammonium hydroxide (TMAOH) (25% aq. solution), and sodium hydroxide pellets (NaOH) (Baker Analyzed) were used. AOT was further purified before use.[22]

Preparation of Micellar solutions: The micellar solutions were prepared by the phase transfer method, which involves equilibrating a solution of surfactant in a hydrocarbon solvent with an aqueous solution containing the electrolytes of interest, followed by separation of phases. Three solutions were prepared: 0.065 M AOT in n-hexane, 0.2 M $Zn(NO_3)_2$ aqueous solution, and 0.5 M H_3PO_4, 0.24 M NaOH and 0.93 M of TMAOH as another aqueous solution. The zinc and phosphate micelle solutions were prepared by mixing 8 ml of the aqueous solutions with 200 ml of the n-hexane solution in two separate containers. After shaking the mixtures for a minute, the solutions were equilibrated for 48 hours, centrifuged and the remaining aqueous phases were removed from the hexane. The micellar solutions were allowed to age for up to three weeks.

Preparation of zincophosphates: The zinc and phosphate containing micellar solutions, aged for different times were mixed in various volume proportions as outlined in the text. The reactions were carried out at 25°C.

Characterization of micelle solutions and solid zincophosphates:

Elemental analysis was done by inductively coupled plasma spectroscopy and combustion methods. Micelle size and particle growth were monitored by quasi elastic light scattering. These experiments were carried out using a digital correlator from Brookhaven Instruments (BI-200 SM) with an Excel 3000 argon-ion laser operating at 514.5 nm. All experiments were performed at 25°C with a laser power of 200 mW at a scattering angle of 90°. Prior to light scattering experiments, dust particles were filtered out from the micellar solutions using 0.2 μm Nylon 66 membrane filters. Using software supplied by the vendor, particle sizes were obtained by using the method of cumulants and exponential sampling analysis. ^{31}P NMR spectra of the phosphate micelle solutions were recorded at 121 MHz with a Bruker MSL-300 NMR spectrometer at room temperature. External phosphoric acid (0.5M) was used as the reference. X-ray powder patterns were determined with a X-ray diffractometer (Rigaku, D-Max-2B) using nickel-filtered Cu Kα (λ=1.5405 Å) radiation. Particle size and morphology were determined by scanning electron microscopy (SEM) (Hitachi S-4000). Morphology and selected area diffraction at early stages of particle growth were obtained using transmission electron microscopy using either a Hitachi (H-9000 NAR) with 1.8Å resolution at a voltage of 300 kV or Philips (CM-200) with 2.7Å resolution and an accelerating voltage of 200 kV. Only with the latter instrument could we obtain selected area diffraction, because of minimized beam damage. Non contact AFM measurements were made on a Nanoscope III Scanning Probe Microscope (Digital Instruments) or an Autoprobe LS (Park Instruments).

Results

Conventional Synthesis :

Stucky and coworkers have reported detailed studies of the crystallization of zincophosphates from zinc and phosphate containing solutions.[21] Since our goal in this study was to examine the crystallization of zincophosphate sodalite, we repeated their procedure for this framework over the pH range of 6.6 to 7.6. In all cases, the observations were similar. There was the immediate formation of a white precipitate and the gel settled out of the reaction mixture within 2 hours. The product was removed after four hours and in all cases was sodalite, with the characteristic diffraction pattern and morphology shown in Figure 1.

Preparation and properties of Reverse Micelles :

(a) Zinc containing micelle: The aqueous solutions in equilibrium with the n-hexane phase were analyzed for Zn, Na, N, and from these results, the uptake of reactants into the micelle was calculated. Water content of hexane was determined by Karl-Fisher titration. These data are summarized in Table 1. Light scattering experiments show that the diameter of the zinc containing micelle is 8.5 nm. The variation in size over a three week period is plotted in Figure 2. There was minimal change in size over this time period. Considering the $[H_2O]/[AOT]$ (w) ratio of 13, the zinc micelles are considerably larger than micelles containing comparable levels of only water.[17]

For transition metals, e.g. Cu^{2+} in reverse micelles, above a w of 10, the ions were found to be totally hydrated and bulk water is present.[17a] A similar situation can be expected in these zinc micelles.

(b) Phosphate containing micelle: From the elemental analysis (Na, P, N, C) of the aqueous phosphate solution after equilibration, the micellar composition was estimated and is shown in Table 1. Tetramethylammonium ions were necessary for the uptake of phosphate ions into the micelle. There is a change in size of the phosphate micelle from 15 to 19 nm over a three week period (Figure 2). Measurement of pH with a glass electrode showed that the initial solution had a pH of 11.4 and gradually decreased in time to a pH of 9.6 after 21 days. Even though pH values measured in a hydrocarbon environment may not be directly comparable with aqueous solutions,[16] the trend is that the solution is becoming less basic with time. Another method discussed in the literature for estimating intramicellar pH is ^{31}P NMR.[23] ^{31}P NMR spectra of the phosphate micellar solutions as a function of aging time is shown in Figure 3. Chemical shift values are quoted relative to a phosphoric acid standard of 0 ppm. A series of phosphate buffers were used to correlate the chemical shift with the pH. The assumption being made here is that the pK_a's of phosphoric acid remain unchanged in the micelle.[23] With this calibration, the intramicellar pH was found to decrease from 12.3 to 11.8 over 21 days, the same trend as measured with the glass electrode.

Zincophosphates formed by reaction of zinc and phosphate micelles:

There are three sets of experiments that we report here using the zinc and phosphate micelles. First, we report on the nature of solids formed by mixing equal volumes of zinc and phosphate micelle, both solutions being aged for periods of time varying from 0 to 13 days. Second, we report an experiment in which the volume of zinc micelle was three times that of the phosphate micelle (both samples aged for 8 days). The results from these experiments are summarized in Table 2. Third, we focus on reactions between zinc and phosphate micelles aged for 8 days and mixed with volume ratios of 0.8 to 1.2.

For the experiments reported in Table 2, the solutions were clear upon mixing the micelles. Then at various times as indicated in the table, it was noted that a white product began settling out. After completion of the settling process, the product was removed, washed and analyzed by powder X-ray diffraction and the results are shown in Figure 4. The product recovered with the micelle solutions aged for 2 days of reaction is a mixture of hexagonal sodium zinc phosphate and sodalite.[21b] Sodalite is formed when the micelles were aged for more than 6 days. The product formed upon mixing 120 ml of zinc micelle solution with 40 ml phosphate micelle solution leads to the formation of hoepite (zinc phosphate)[21b], as shown in Figure 4c. In Figure 5 are shown the ^{31}P NMR spectra of the solutions from which hexagonal zinc phosphate plus sodalite, sodalite and hoepite were obtained, and indicates that the acidity of these solutions are increasing.

Formation of Sodalite

In order to further explore crystal growth, we focused on the composition and conditions shown in Table 2 that resulted in sodalite formation. Sodalite is a member of the microporous family of frameworks and has been extensively studied in the aluminosilicate[24] as well as all silica systems.[25]

(a) Micellar Compositions: Solutions of phosphate and zinc micelle aged for 8 days were used as starting materials for sodalite synthesis. We examined the solids formed upon mixing these solutions in different volume ratios. Based on these results, three compositions made by adjusting the relative ratios of the zinc and the phosphate micelle solutions between 0.8 and 1.2 were examined in more detail. In Table 3, these are identified as compositions A, B and C. The concentrations of the number of micelles was calculated based on their size by the formalism presented by Towey et al.[26]

^{31}P NMR of the solutions corresponding to compositions A, B and C are shown in Figure 6. With increasing content of the zinc micelle, the overall solution becomes more acidic. From the pH-NMR calibration data, the pH values in compositions A, B and C are 7.6, 7.2 and 6.8, respectively.

(b) Particle Growth Characteristics: There was a marked difference in the rates of appearance of particles for the three compositions. In the case of composition A, the solution did not turn cloudy and particles appeared at the bottom of the reaction chamber after 2 days and increased with time over 4 days. For composition B, the reactor became cloudy within the first 12 hours, followed by settling out of particles over the next 24 hours. For composition C, the solution became cloudy within an

hour and particles mostly settled out in 4 hours.

Laser light scattering obtained on all three compositions upon mixing the zinc and phosphate micelles indicated that the initial micelle size is of the order of 15-50 nm. However, the nature of the particle growth varied significantly between the three compositions. Before we present the data obtained by light scattering, a word of caution is in order. It is evident from the light scattering literature that analysis of the autocorrelation function for size distribution in polydisperse systems is complicated. In order to choose the appropriate method for data analysis, we obtained polystyrene standards of 16, 65, 445 and 944 nm. With the software involving the method of cumulants, reasonable values within 10% of the size could be readily obtained. However, when we took mixtures of two standards, the exponential sampling technique did a better job. For example, using the exponential method, a mixture of 16 and 65 nm particles were analyzed and indicated a bimodal distribution of 28 and 56 nm. Considering that the micelles are growing in size to form the zincophosphate particles, polydispersity is expected. So, we used the exponential sampling method to derive particle size. For most samples we examined, two population distributions were calculated, and each is represented in Figure 7 with the appropriate range. The trends observed using the method of cumulants or the mean size (first moment) obtained by the exponential sampling method were similar.

It is evident from Figure 7 that the time scale on the x-axis is changing from days to hours to minutes as we go from compositions A through C. The sizes shown in Figure 7 are used here to indicate trends in particle growth.

For compositions B and C, there is a period of time in which the particle size remains below 100 nm, followed by a rapid increase. However, the period of time before the growth spurt is very different, about 16 hours for Composition B and less than 2 hours for Composition C, consistent with our visual observations. In the case of composition A, the growth seems more complicated. There is no growth spurt, rather a gradual increase, which reaches a maximum around 36 hours, followed by a decrease and then further growth. As mentioned earlier, we did not notice any cloudiness during the growth, only settled particles. Combining this information with the light scattering, we suggest that a small number of particles grow to a certain size, settle out and are replaced in solution by new particles.

(c) Diffraction patterns of the recovered Particles: For composition A, the solution remains clear and evidence of reaction is provided by solids appearing at the bottom of the reaction vessel for the first time after 2 days. Figure 8 shows the diffraction patterns obtained from this sample. The peaks due to sodalite are evident. This shows that the settled particles are already crystalline, implying that crystal growth is occurring while suspended. With time, the crystals increase in amount and are characteristic of the sodalite framework (Figure 8b). For composition B, as soon as the solution became cloudy, it was centrifuged. This typically took about 12-16 hours. The diffraction pattern of this solid is characteristic of the sodalite framework, as shown in Figure 9a (the amount of sample collected at this stage is very small, which accounts for the poorer quality of diffraction patterns). The crystals recovered from the bottom of the chamber after settling for 24 hours also exhibit the sodalite crystal

patterns (Figure 9b). For composition C, examination of the particles formed immediately after the appearance of turbidity are mostly amorphous by diffraction. (Figure 10a). The settled amorphous solid was monitored by diffraction and transforms to sodalite over a 4-day period, as shown by the diffraction patterns in Figures 10b and 10c.

(d) Microscopy of the Recovered Particles : Electron microscopy was used to examine the morphology of the solids formed with each composition. Figure 11a shows the scanning electron micrograph of the crystals obtained after settling (4 days) for composition A. The sizes of these crystals are between 500-600 nm. The morphologies are cubic crystals, or pyramids (half-cubes). Centrifugation of the reaction mixture after 18 hours of reaction did afford a small quantity of solid, which was examined by TEM and shown in Figure 11b. Clearly, the morphology of the crystals is similar to that observed after 2 days, though the crystals appear to be smaller (100-500nm), and peaked between 200-220 nm. Selected area diffraction of the crystal shows that the material is crystalline. Thus, it appears that at all observable stages of growth, the morphology of the sodalite crystals remain similar, with size and yield increasing in time.

The surfaces of (100) faces of a cubic sodalite crystal were examined by non-contact atomic force microscopy (AFM). Figure 12 shows the micrograph of the surface for two different crystals. There appear to be flat terraces followed by steps, roughly aligned with the crystal side. The step heights (Figure 12a) were about 10Å in height, corresponding to a sodalite cage. On some crystal surfaces, e.g. the one

shown in Figure 12b, there was a distribution of step heights, with the smallest steps being 10 Å, but there were steps also as large as 30Å.

Figure 13a show SEM pictures of the particles obtained for composition B before settling. The suspended particles are crystallites of sizes less than 600 nm and eventually aggregate to form the 2-3 μm settled crystals (not shown). Solids were recovered after 6 hours of reaction (prior to appearance of any cloudiness) by centrifugation and examined by TEM and is shown in Figure 13b. There is clearly evidence of aggregates of small particles. The selected area diffraction show that this material is crystalline.

The transmission electron micrograph shown in Figure 14a are for particles collected from the turbid solution prior to settling for Composition C . These are discrete particles of approximately 5 μm. These particles settle, agglomerate and form a contiguous solid with time, whose SEM picture is shown in Figure 14b. Sodalite crystals grow out of this settled solid phase, with the morphology shown in Figure 14c after 4 days of growth.

It was of interest to determine if in composition C, sodalite crystal growth from the suspended particles is possible. The problem is that these particles settle out within a few hours. Thus, it was necessary to develop a strategy for keeping these particles suspended without altering the chemical composition. It has been reported in the literature that the particles in a fluid which will sediment due to gravitational forces (Stokes law) can be kept suspended by rotation of the reaction chamber.[27] We constructed a system which accommodated the cylindrical Teflon bottles typically

used in the synthesis. A schematic of this equipment is shown in Figure 15a. The reactor rotates around its central axis at speeds up to 7 to 45 rpm. The orbits assumed by the particles are approximate circles around a center displaced horizontally from the axis of rotation. A minimum rotation speed is required in order to insure that this center lies within the dimensions of the reactor. At very high rotation rates, particles with densities higher than the fluid (as in this case) will spiral out and hit the wall of the reactor. The choice of the rotation speed thus needs to be optimized depending on the particle-fluid system.

Formation of sodalite crystals by pathway C could be completed in the rotating cell at 11 rpm with minimal sedimentation on the walls of the reactor over a period of 10 days. From the individual amorphous particles, sodalite crystals were seen to grow, as shown in Figure 15b.

DISCUSSION

Results above show that it is possible to grow zincophosphate frameworks from reactants initially contained in reverse micelles. We discuss the role of the reverse micelle, with particular emphasis on the structure and speciation of the zinc and phosphate species and their interactions to form the solid phases. Correlation of the micellar chemistry with the well-known aqueous chemistry also serves to distinguish the role of the reverse micelle. In particular, the marked difference in particle growth rates and morphologies of sodalite crystals formed by minor changes

of composition is interesting. Understanding these observations provides information on the mechanism of the crystallization process.

Nature of Reverse Micelles:

The procedure of phase transfer to form reverse micelles by equilibrating an AOT-hydrocarbon with an aqueous salt solution is well studied in the literature.[28] From Table 1, it is evident that considerable amounts of water are taken up into the zinc and phosphate micelles. Considering that the water/AOT ratios of the two micelles (13 and 21) are considerably higher than that necessary for hydration of sulfonate groups, bulk water must be present in the pools.[29] As the water becomes more bulk-like, the ions present in the micelles also have relatively unrestricted motion.[30]

Water content of phosphate micelles is higher than the zinc micelles. The amount of water taken up in a micelle is strongly dependent on the salt concentration.[31] In the case of the phosphate micelle, this is a basic solution. Previous studies on uptake of basic solutions such as ammonium hydroxide into AOT micelles show that considerable amounts of water are incorporated into the reverse micelle, a factor of three greater compared to uptake of Fe^{3+} ion.[32] Highly basic solutions have also been made with aqueous ammonia in the water pools of AOT micelles for hydrolysis of alkoxides to make silica. Based on the size of the silica particles created, it was postulated that the high pH caused an increase in diameter of the water pools.[33] Phosphate micelles also contain higher content of solutes, in particular, TMA cation. Large amounts of TMA can be solubilized in reverse micelles because of the weak interaction with the head groups of the surfactant.[31]

Also, in the case of phosphate micelle, an upfield shift of the ^{31}P NMR signal was noted with aging, indicating that the micelle is becoming less basic with time. This behavior can be understood from the acid-base chemistry that can occur inside the micelle. Along with the phosphate, Na^+ and TMA^+ ions, OH^- ions are also transported into the micelle from the aqueous solution. The head-group of the detergent (AOT) is a succinate ester. It has been reported in the literature that in the presence of base, the following hydrolysis reaction can take place:[34]

$$OH^- + -CH_2COOR \rightarrow -CH_2COO^- + ROH$$

This leads to a decrease of pH in the micelle and the phosphate species reequilibrate. The reverse micellar structure appears to be maintained. Hydrolysis upon aging is providing a mechanism to change the intramicellar pH and the phosphate species.

Studies based on the acid-sensitive optical probe 2,7-dichlorofluorescein and the hydrolysis of triethyl orthobenzoate ester suggest that the zinc micelle might be somewhat acidic.[35] This is probably not surprising considering the hydrolysis of aquated zinc ions.[36]

Comparison of zincophosphates made from reverse micelles and conventional synthesis:

In the experiments described in Table 1 we start with the same set of reactants. Aging decreases the pH in the phosphate micelle and the contents of the zinc micelle are acidic. Mixing these two micelles results in a more acidic solution. From the

intramicellar NMR data, it appears that the hexagonal sodium zinc phosphate, sodalite and hoepite are formed from micellar solutions with increasing acidity. Stucky et al. have examined the various phases formed with zincophosphates from purely aqueous medium as a function of pH. They noted that hexagonal sodium zinc phosphate is formed at high pH range (pH = 10) and sodalite is formed at neutral pH (pH = 7) and hoepite is formed at acidic pH's.[21] It is clear from these trends that the overall chemistry regarding the formation of zincophosphate crystalline phases starting with reactants in micellar phases are similar to that in aqueous solution. This establishes that the micellar and aqueous chemistry follow similar pathways.

Focusing now on the crystallization of the sodalite zincophosphate, we find that by varying the zinc to phosphate micellar volume ratios between 0.8 and 1.2, sodalite growth rates vary over a wide range. ^{31}P NMR studies of compositions A,B and C show that at the beginning of the reaction, the intramicellar pH's are 7.5, 7.2 and 6.8, respectively. As shown earlier (Figure 1), under these pH conditions, there was no discernible difference in the growth of sodalite in the conventional system. We note here again that in deriving the intramicellar pH's, we have made the assumption that the pK_a's of phosphoric acid remain unchanged in the micellar environment. With this caveat in mind, it appears that the crystallization dynamics in the micellar system is distinct from the conventional system.

For composition A, crystals appear after two days and continually increase with time. The powder XRD pattern as well as electron microscopy confirms that sodalite is being formed while suspended, without any detectable intermediate amorphous

phase. Light scattering studies indicate continuous growth in size. Once particles reach a certain size, they sediment and stop growing. At the same time, smaller particles in the reaction mixture grow larger resulting in more product. The morphology of the crystal suggests that the crystals are growing by deposition along specific crystal planes proceeding towards a cubic structure.

In the case for composition B, crystals appear within 12-16 hours again without any apparent intermediate amorphous phase. The crystals recovered from the bottom of the chamber after settling have similar particle size and morphologies as the suspended particles, except that they appear agglomerated. The TEM micrograph at the early stages show agglomerated particles. Light scattering suggests that the rapid growth of particles only occur after they reach a size of 75 nm.

For composition C, crystals appear after 4 days and are clearly emerging from a settled amorphous phase. This pathway is marked by the rapidity of the initial reaction to form amorphous zincophosphates- the reactant mixture turns turbid in 1 hour, and complete settling of the solid is found in 4 hours. The growth pattern as measured by light scattering for composition C is consistent with these observations.

The reverse micellar environment:

Thus, it is clear that the micellar environment is playing a major role in the kinetics of the crystal growth process, though the overall framework is the same as in conventional synthesis. There are several ways that the reverse micelle can influence particle growth.

a) Micellar Dynamics: The interaction between the zinc and phosphate species is controlled by micellar dynamics. Micelles move by Brownian diffusive motion and collide with rate constants of $\sim 10^6$-10^8 liter mol^{-1} s^{-1} [37]. During these collisions, brief fusions of micelles occur lasting for microseconds. It provides enough time for exchange of water pools and thereby the reactants enclosed in them.[38] Large cations and anions, such as $Ru(bpy)_3^{2+}$, methylviologen and $Fe(CN)_6^{3-}$ are known to interchange between water pools.[39]

The exchange rates of aqueous solubilisates between water droplets in AOT reverse micelles depends on the number of micelles, water content, and hence the droplet size. Similarity of the water/AOT ratio and droplet concentrations of compositions A-C imply that these are not controlling factors in the growth process. Considering the high water content of the zinc and phosphate micelles and the similarity of sizes, rapid exchange of electrolytes upon collision is expected, as noted for other electrolyte systems in reverse micelles.[40] This equilibration should take place on millisecond time scales. Considering that the particle growth process is at least of the order of an hour, the reactant composition in the micelles should be in a state of equilibrium. The water layer in the micelles can be considered to be a pseudocontinuous phase and the growth kinetics should be dependent on the intramicellar concentration of the reactant species.[37] In this system, such exchange leads to a wide distribution of zinc, phosphate and hydroxide species i.e. xZn,yPO_4,zOH in the micelles, resulting in a considerable heterogeneous population of micellar contents.

b) Compositional differences: From Table 3, we note that the number of zinc micelles always exceeds the number of phosphate micelles, but the relative ratio gradually increases from 3 in composition A to 4.5 in composition C. The other major difference is the intramicellar pH, as discussed above.

c)Nucleating Species: The driving force for nucleation is dependent on the degree of supersaturation of the appropriate nucleating species. The nature of the nucleating species in many crystallization reactions is not obvious. For example, in the precipitation of Ag_2WO_4 , it is not WO_4^{2-}, but rather intermediate species such as $W_6O_{21}^{2-}$, $W_{12}O_{41}^{10-}$, $HW_6O_{21}^{5-}$.[41] The same is true for formation of ferric hydroxide, in which the important reaction is between $Fe_9(OH)_{20}^{7+}$ and $Fe_3(OH)_4^{4+}$, rather than between Fe^{3+} and $3OH^-$.[42] Complicated reactions involving polymeric nucleating intermediates have been proposed for formation of TiO_2, $Cr(OH)_3$ and $Mg(OH)_2$.[13]

Also, the role of pH on nucleating species is well recognized in many crystallization processes. Drastic effects of pH on supersaturation and the consequent alteration of the growth rate is known for calcium hydrogen phosphates.[43] The hydroxide and phosphate ion concentrations appear in the ion product $[Ca^{2+}]^{10}[PO_4^{3-}]^6[OH^-]^2$ as exponents and slight increase of pH considerably increases the supersaturation. Thus, a change in pH from 7.4 to 7.8 resulted in considerable increase of crystal growth rates. Indeed, above a pH of 7.8, it was difficult to prepare a supersaturated solution without spontaneous precipitation of calcium phosphate.[43] For $Cr(OH)_3$, an amorphous precipitate is formed at pH below 10, whereas a crystalline material is formed at pH above 10.[44]

In accordance with these earlier studies in aqueous systems, we propose that the intramicellar pH is influencing the concentration of nucleating species responsible for formation of zincophosphate sodalite. Thus, in all three compositions (A-C), homogeneous nucleation is beginning in the micelle, and since the supersaturation of the nucleating species is varying, there is a wide range of nucleation rates. Even though the structure of the nucleating species is not identified, the necessity of hydrolysis of the Zn-O-P bond in their formation is recognized. Hydrolysis reactions have been noted in reverse micelles. Base catalyzed hydrolysis of esters,[45a] as well as the formation of ferric oxyhydroxide species by hydrolysis of ferric ammonium sulphate has been reported.[45b] Hydrolysis of alkoxides in micelles have shown that the concentration of the reactants and water determine supersaturation levels.[45c] The chemistry involved in crystallization of sodalite is probably more complicated than these examples, but of similar origin.

Mechanisms of Zincophosphate Sodalite Growth:

In composition A, where the supersaturation is the lowest, crystal growth proceeds slowly, controlled by surface attachment kinetics. We consider the surface morphology indicated by AFM to be evidence for a layer-by-layer growth,[46] and is consistent with the cubic morphology observed by SEM. It is known that at low supersaturation, crystals of compact shapes are formed, since the minimum overall energy of the crystal surface is reached under very slow growth , equilibrium-like conditions.[47]

The growth process in Pathway B can be analyzed as an aggregation process. The early morphology of these crystals appears cubic in nature, suggesting that the initial growth process may be similar to that of composition A. The viable nuclei formed grow by incorporating other nuclei. The mobility of the nuclei by diffusion and convection contribute to the aggregation process. Such diffusion controlled micellar collisions have been proposed for growth of silica and carbonate particles[18c,d] The size that nuclei will have to reach before aggregation begins is of interest. Since Pathway B results in direct formation of crystals from nuclei, particle size analysis during this crystal growth process provides this opportunity. The TEM picture in Figure 13b shows aggregates of particles. The approximate size of these crystallites is difficult to determine, but light scattering indicates a size of 75 nm before rapid growth ensues.

The differences in crystal growth rates between compositions A and B are being assigned to the differences in micellar pH, which leads to two effects. First, it alters the concentration of solution species. Lazic has recently reported a reduction of the induction period in hydroxyapatite formation from amorphous calcium phosphate as a function of pH.[48] Beyond pH 10.2, the decrease in induction period was correlated with deprotonation of HPO_4^{2-} and the increase in concentration of $CaPO_4^-$. The second effect of pH on crystal growth arises from the surface charge on the particle. For example, with both $CaHPO_4.2H_2O$ and hydroxyapatite, crystals grow slower at pH values less than the pH corresponding to the point of zero charge.[49] This was interpreted as the charge on the crystal face being important in building of growth units in the lattice.

In pathway C, the intra-micellar conditions result in higher supersaturation. This leads to rapid nucleation, and since the induction time for crystal formation is longer, amorphous particles are formed. The morphology of the particles formed initially in composition C supports the high supersaturation hypothesis. If the rate of particle growth is very high, then the heat of precipitation cannot be transferred efficiently into solution. This leads to convection and the particle is surrounded by depleted regions. The particle extends its surface highly anisotropically. This leads to structures shown in Figures 14a and 15b.

The formation of an amorphous phase in systems with high supersaturation has been noted in crystallization of $CaCO_3$, with the amorphous phase transforming finally to vaterite and then calcite.[50] Similarly, hydroxyapatite and $Mg(OH)_2$ forms an amorphous phase followed by crystallization.[51] In the case of $Al(OH)_3$, an amorphous precipitate transforms to pseudoboehmite.[52] The explanation for these observations is that the nuclei formed from highly supersaturated solutions do not have an exactly defined structure and the structure that is formed is determined only during the later stages of the precipitation. Crystals are formed from these amorphous materials by dissolution into the mother liquor,[11,13] and thereby providing nutrients to the more stable phase by a solution mediated transformation. However, in the present case, nutrients cannot dissolve in the organic medium. There are two possibilities. Direct transformation in the solid state, as has been reported for transformation of vaterite to calcite. In this case, the morphology remained unchanged upon transformation,[50] and is not consistent with the present observations. The second possibility stems from

previous studies on precipitation of metal hydroxides, which have shown that considerable amount of non-structural water that is retained in the precipitate can be liberated during the aging process.[53] Thus after settling of the amorphous zincophosphate, with time, it is surrounded by a thin water layer that can transport nutrients. Such a mechanism is supported by the rotating cell experiment, in which the suspended amorphous particles transform directly to sodalite crystals. The gel particles appear to act as epitaxial sites for growth, as seen in Figure 15. This process must occur by solid dissolution and surface transport to the growing crystal via the water layer.

Role of reverse micelle:

The reverse micelle is providing the control on supersaturation by minor changes in intra-micellar reactant composition. Aqueous solutions at pH's comparable to that in the reverse micelles show no apparent difference in the crystallization pathways. The question that arises is why and how the reverse micelles allow this level of control. We explain these observations as follows. In the micellar system, after the micelles have equilibrated, there is a wide distribution of zinc, phosphate and hydroxide ion occupancies in the different micelles. Depending on these intramicellar concentrations, there will be a fraction of these micelles in which saturation conditions will be exceeded. This fraction increases as the composition changes from A to C. However, only in those micelles in which supersaturation conditions exist will particle formation occur. Once a nucleus is formed, growth is controlled by transport of

species to the surface and surface integration. This is dependent on the collision of the growing particle with micelles containing soluble species or other nucleated particles. For composition A, where there are few nuclei formed in the micelles, the growth will have to occur by acceptance of solution species present in other micelles. Since the nuclei can no longer be considered micelles, the intermicellar exchange where micelles upon collision open up a conduit to exchange solution species is no longer possible. Thus, growth of these particles by accepting solution species from other micelles will be slow. For composition C on the other extreme, the particles grow rapidly by aggregation. Increased aggregation with supersaturation has been noted for silver clusters in AOT micelles.[54] Composition B represents an intermediate situation, where more particles are formed, and there is enough time prior to aggregation to form sodalite nuclei.

In the conventional aqueous systems, where there exists uniformity of compositions throughout the system, it is much more difficult to control the supersaturation levels, as noted here for reverse micellar systems.

Conclusions

This study shows that it is possible to make complicated structures, such as zincophosphate sodalite from reactants contained in reverse micelles. Overall, the reaction chemistry followed the conventional aqueous hydrothermal chemistry. The internal pH's of the micelles could be controlled with aging. The important discovery, as contrasted to the aqueous system, is that it was possible to control the crystal

growth kinetics by using reverse micelles. At low supersaturation levels, crystal growth by a layer growth mechanism resulting in ideal cubic crystals was observed. At high supersaturation, crystal growth occurred from amorphous agglomerates, much like in conventional synthesis. At intermediate supersaturation, a nuclei aggregation process was observed.

Acknowledgements

We sincerely acknowledge the help of Dr. Charles Kresge for the elemental analysis and many useful discussions. In addition, the help of Dr. Dale Karewik, Mr. David Frate and Mr. Tom Hickey in assembling the rotating cell are acknowledged. We also thank Digital Instruments for doing an AFM study. Funding for this work was provided by NASA. Dr. Suh acknowledges the continuing support of NRC and NASA Lewis Research Center.

Table 1: Composition of Micellar solutions:

Zn-micelle	P-micelle
$[Zn^{2+}]$ = 0.0075 M	[Phosphate] = 0.0125 M
$[Na^{+}]$ = 0.0525 M	$[Na^{+}]$ = 0.055 M
$[NO_3^{-}]$ = 0.00507 M	$[TMA^{+}]$ = 0.346 M
[AOT] = 0.065 M	[AOT] = 0.065 M
$[H_2O]/[AOT]$ = 13	$[H_2O]/[AOT]$ = 21
Micelle size = 8.5 $\pm$ 1 nm	Micelle size = 15 $\pm$ 1 nm

Table 2: Frameworks formed by mixing zinc and phosphate micelles.

$Zn:PO_4$ (volume)	Equilibration time (days)	Initial appearance of product (days)	Product formation completed (days)	Final product (XRD)
1:1	0	7	9	unknown + sodalite
1:1	2	5	6	hexagonal zinc phosphate + sodalite
1:1	6	1	1.5	sodalite
1:1	8	0.5-1	0.75-2	sodalite
1:1	10	0.5-1	0.75-1.5	sodalite
1:1	13	0.5	0.75-1	sodalite
3:1	8	1	2	hoepite

Table 3: Characteristics of Sodalite forming compositions.

Composition	Reaction volume (ml)		concentration (moles)		Number of Droplets (moles)	
	Zn micelle	Phosphate Micelle	Zinc ions	Phosphate ions	Zn micelle	Phosphate micelle
A	40	50	3×10^{-4}	6.25×10^{-4}	4×10^{-5}	1.35×10^{-5}
B	40	40	3×10^{-4}	5×10^{-4}	4×10^{-5}	1.1×10^{-5}
C	50	40	3.8×10^{-4}	5×10^{-4}	5×10^{-5}	1.1×10^{-5}

References

1. Szostak, R. Handbook of Molecular Sieves, Van Nostrand, 1992.

2. Zeolites and Related Microporous Materials: State of the Art 1994, Eds. Weitkamp, J.; Karge, H.G.; Pfeifer, H.; Holderich, W., Elsevier, Amsterdam, 1994.

3. Geus, E.R. den Exter, M.J.; van Bekkum, H. J. Chem. Soc. Faraday Trans. **1992**, 88, 3101.

4. Smolka, H.G.; Schwuger, M.J. Colloid Polym. Sci. **1978**, 256, 270.

5. Ward, J.W. Applied Industrial Catalysis, **1984**, 3, 271

6. Davis, M.E.; Lobo R.F. Chem. Mater. **1992** 4, 756.

7. Breck, D.W. Zeolite Molecular Sieves, John-Wiley, NY, 1974.

8. Dutta, P.K., J. Incl. Phenom. Molec. Recog. Chem. **1995**, 21, 215.

9. (a) McCormick, A.V.; Bell, A.T. Catal. Rev.-Sci. Eng. **1989**, 31, 97.

   (b) Burkett, S. L.; Davis, M.E. J. Phys. Chem. **1994**, 98, 4647.

10. Iton, L.E.; Trouw, F.; Brun, T.O.; Epperson, J.E.; White, J.W.; Henderson, S.J. Langmuir, **1992**, 8, 1045.

11. Mullin, J.W., Crystallization, Butterworth-Heinemann, London, 1993.

12. Walton, A.G., Dispersion of Powder in Liquids, Ed. Parfitt, G.D., p 175, Appl. Sci. Publ. London, 1973.

13. Sohnel, O.; Garside, J. Preceipitation-Basic Principles and Industrail Application, Butterworth-Heinemann, London, 1992.

14. Kirkova, E.; Djarova, M. Industrial Crystallization 78 Eds. Jancic, S.J.; deJong, E.J. p 81, North-Holland, Amsterdam, 1979.

15. Furedi-Milhofer, H.; Oljica-Zabcic, E.; Purgaric, B.; Kosar-Grasic, B.; Parkovic, N. J. Inorg. Nucl. Chem. **1975**, 37, 2047.

16. Menger, F.M.; Yamada, K. J. Am. Chem. Soc. **1979**, 101, 6731.

17. (a) Pileni, M.P. J. Phys. Chem. **1993**, 97, 6961.
(b) Fendler, J.H. Chem. Rev. **1987**, 87, 877.

18. (a) Steigerwald, M.L.; Alivisatos, A.P.; Gibson, J.M.; Harris, t.D.; Kortan, R.; Muller, A.J.; Thayer, A.M. Duncan, T.M.; Douglas, D.C.; Brus, L.E. J. Am. Chem. Soc. **1988**, 110, 3046.

(b) Boutonnet, M.; Kizling, J.; Stenius, P. Colloids Surfaces, **1982**, 5, 209.
(c) Osseo-Asare, K.; Arriagada, I.J. Colloids and Surfaces, **1990**, 50, 321.
(d) Kandori, K.; Kon-no, K.; Kitaharo, A.J. Dispersion Sci. Technol. **1988**, 9, 61.

19. (a) Dutta, P.K.; Robins, D. Langmuir, **1991**, 7, 1048.
(b) Dutta, P.K.; Reddy, K.S.N.; Salvati, L.; Jakupca, M. Nature, **1995**, 374, 44.

20. Lang, J.; Jada, A.; Malliaris, A. J. Phys. Chem. **1988**, 92, 1946.

21. (a) Gier, T.E.; Stucky, G.D. Nature, **1991**, 349, 508.
(b) Gier, T.E.; Harrison, T.A.; Nenoff, T.M.; Stucky, G.D. in Molecular Sieves, Ed. Occelli, M.L.; Robson, H. p. 407, Van Nostrand Reinhold, N.Y. 1992.
(c) Nenoff, T.M.; Harrison, W.T.A.; Gier, T.E.; Stucky, G.D. J. Am. Chem. Soc. (1991), 113, 378.

22. Martin, C. A.; Magid, L. J. J. Phys. Chem. **1981,** 85 , 3938.

23. (a) Fujii, H.; Kawai, T.; Nishikawa, H.; Ebert, G. Colloid Polymer Sci. **1982**, 260, 697.
(b) Smith, R.E.; Luisi, P.L. Helv. Chim. Acta. **1980**, 63, 2302.

24. Felsche, J.; Luger, S.; Baerlocher, C. Zeolites **1986**, 6, 637.

25. Bibby, D.M.; Dale, M.P. Nature, **1985**, 317, 157.

26. Towey, T.F.; Khan-Lodhi, A.; Robinson, B.H. J. Chem. Soc. Faraday Trans. **1990**, 86, 3757.

27. (a) Roberts, G.O.; Kornfeld, D.M.; Fowlis, W.W. J. Fluid Mech. **1991**, 229, 555.
(b) Cleland, J.G.; Kornfeld, D.M. Trans. ASME, **1992**, 114, 616.

28. (a) Leodidis, E.B.; Hatton, T.A. Langmuir, **1989**, 5, 741.
(b) Plucinkski, P.; Nitsch, W. Langmuir, **1994**, 10, 371.

29. Karrdori, K.; Kon-No, K.; Kitahara, A. J. Colloid Int. Sci. **1988**, 122, 78.

30. Wong, M.; Thomas, J.K.; Gratzel, M. J. Am. Chem. Soc. **1976**, 98, 2391.

31. Derouiche, A.; Tondre, C. J. Disp. Sci. Technol. **1991**, 12, 517.

32. Gobe, M.; Kon-No, K.; Kandori, K.; Kitahara, A. J. Colloid Int. Sci. **1983**, 93, 293.

33. Yamauchi, H.; Ishikawa, T.; Kondo, S.; Colloids and Surfaces, **1989**, 37, 71.

34. Luisi, P.L. Angew. Chem. Int. Ed. Engl. **1985**, 24, 439.

35. Bardez, E.; Larrey, B.; Zhu, X.X.; Valeur, B. Chem. Phys. Lett. **1990**, 171, 362.

36. Baes, C.F.; Mesmer, R.E. The Hydrolysis of Cations, John-Wiley, NY, 1976.

37. Fletcher, P.D.I.; Howe, A.M.; Robinson, B.H. J. Chem. Soc. Faraday Trans 1, **1987**, 83, 985.

38. Oldfield, C. J. Chem. Soc. Faraday Trans. **1991**, 87, 2607.

39. Modes, S.; Lianos, P. J. Phys. Chem. **1989**, 93, 5854.

40. Eicke, H-F.; Shepherd, J.C.W.; Steinemann, A.; J. Colloid Int. Sci. **1976**, 56, 168.

41. Jensen, J.B.; Lou J.; Acta. Chem. Scand. **1983,** A37, 617.

42. van der Woude, J.H.A.; deBruyn, P.L. Colloids and Surface **1983**, 8, 55.

43. Meyer, J.L.; Nancollas, G.H. Arch. Oral. Biol. **1972**, 17, 1623.

44. Siddiq, M.; Gilanyi, t.; Zettlemoyer, A.C. J. Colloid Int. Sci. **1978**, 64, 192.

45. (a) Menger, F.M.; Donohue, J.A.; Williams, R.F. J. Am. Chem. Soc. **1973**, 95, 286.
(b) Darab, J.G.; Pfund, D.M.; Fulton, J.L.; Linehan, J.C.; Capel, M.; Ma. Y. Langmuir, **1994**, 10, 135.
(c) Hirai, T.; Sato, H.; Komasawa, I.; Ind. Eng. Chem. Res. **1993**, 32, 3014; **1994**, 33, 3262.

46. Schimmel, T.; Winzer, B.; Kemnitzer, R.; Koch, T.; Kuppers, J. Adv. Mater. **1994**, 6, 307.

47. Loades, S.D.; Carr, S.W.; Gay, D.H.; Rohl, A.L. J. Chem. Soc. Chem. Commun. **1994**, 1369.

48. Lazic', S. J. Cryst. Growth **1995**, 147, 147.

49. Hohl, H.; Koutsoukos, P.G.; Nancollas, G.H. J. Cryst. Growth, **1982**, 57, 325.

50. Sohnel, O.; Mullin, J.W. J. Cryst. Growth **1982**, 60, 239.

51. Meyer, J.L. Weatherall, C.C. J. Colloid Interfac Sci. **1982**, 89, 257.

52. Kibalczyc, W.; Melikhov, I.V.; Komarov, V.F. Industrial Crystallization 81, Ed. Jancic, S.J.; deJong, E.J. p 291, North-Holland, Amsterdam, 1982.

53. ref. 13, p 185

54. Petit, C.; Lixon, P.; Pileni, M-P. J. Phys. Chem. **1993**, 97, 12974.

Figure Captions

Figure 1 Diffraction pattern and scanning electron micrograph of zincophosphate sodalite obtained via conventional hydrothermal synthesis.[21]

Figure 2 Size of zinc containing micelle (+) and phosphate containing micelle (△) as a function of time.

Figure 3 ^{31}P NMR signal from phosphate micelle as a function of time.

Figure 4 Powder X-ray diffraction of solids recovered from reaction of zinc and phosphate (1:1 by volume) after aging of micelles for (a) 2 and (b) 8 days. (c)Diffraction pattern of solid recovered from mixing zinc and phosphate micelle (3:1 by volume, aged 8 days).

Figure 5 ^{31}P NMR spectra of solutions obtained by mixing zinc and phosphate micellar solutions (1:1 by volume) after aging for (a) 2 and (b) 8 days (c) zinc and phosphate micelle (3:1 by volume, aged 8 days)

Figure 6 ^{31}P NMR spectra of compositions (a) A (b) B and (c) C.

Figure 7 Particle size distribution as measured by light scattering from compositions (a) A (b) B and (c) C. + and △ represent the smaller and larger sizes, respectively obtained by the exponential sampling method, along with the widths of the distributions.

Figure 8 Diffraction pattern of solids obtained from composition A after (a) 2 and (b) 4 days.

Figure 9 Diffraction pattern of (a) solid recovered as soon as composition B turned cloudy (12 hrs) (b) after solid has settled (36 hrs).

Figure 10 Diffraction pattern of (a) solids recovered at the first sign of turbidity (2 hrs) (b) after 2 days (c) after 4 days.

Figure 11 (a) Scanning electron micrographs of crystals obtained from composition A after 4 days (b) Transmission electron micrograph of crystals obtained from composition A after 18 hours.

Figure 12 Atomic force micrographs of two different crystals obtained from composition A.

Figure 13 Scanning electron micrographs of crystals obtained from composition B at (a) first sign of turbidity (12 hours) (b) Transmission electron micrographs of solid recovered after 8 hours.

Figure 14 Scanning electron micrographs of solids recovered from composition C after (a) 2 hrs (b) 2 days (c) 4 days.

Figure 15 (a) Schematic diagram of the rotation cell (b) Scanning electron micrographs of particle during growth (7 days) from suspended particles using composition C in the rotating cell.

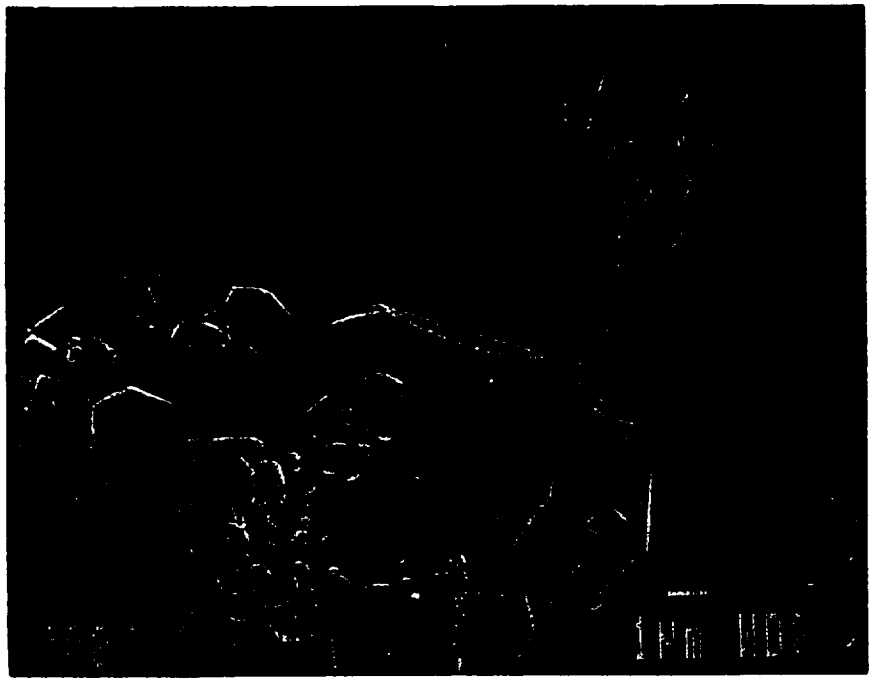

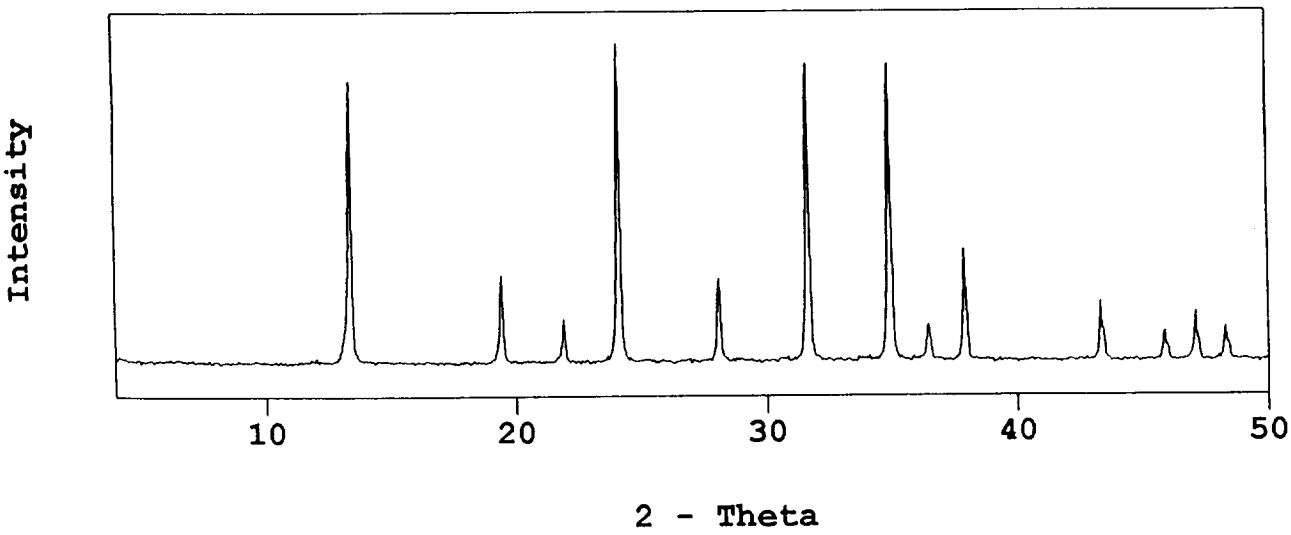
Intensity
10
20
30
40
50
2 - Theta

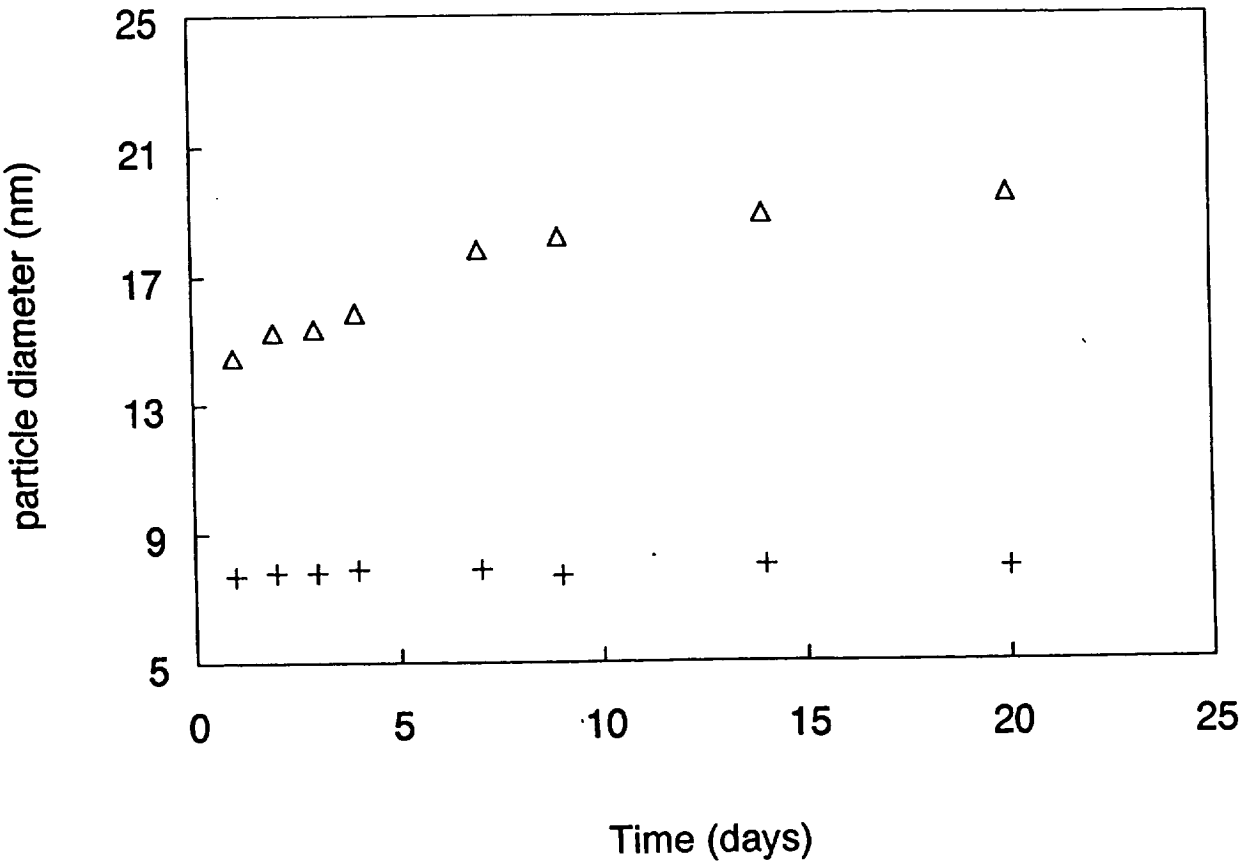
25
21
17
13
9
5
0
5
10
15
20
25
particle diameter (nm)
Time (days)

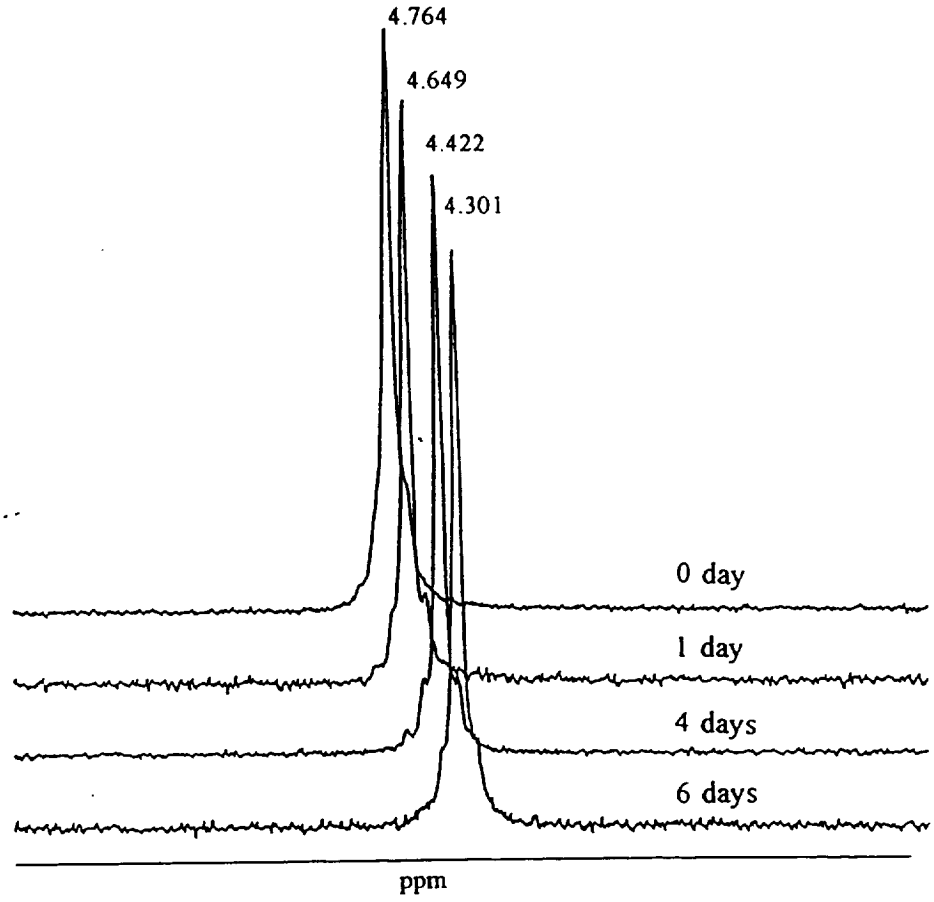
4.764
4.649
4.422
4.301
0 day
1 day
4 days
6 days
ppm

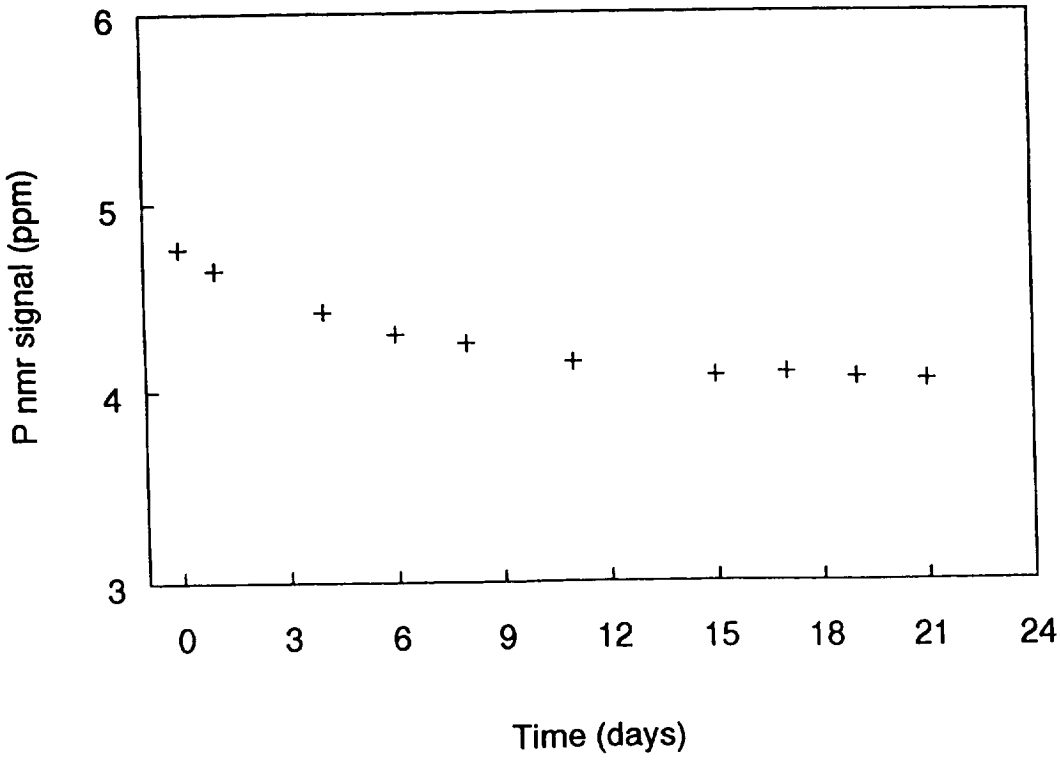
P nmr signal (ppm)
6
5
4
3
0
3
6
9
12
15
18
21
24
Time (days)

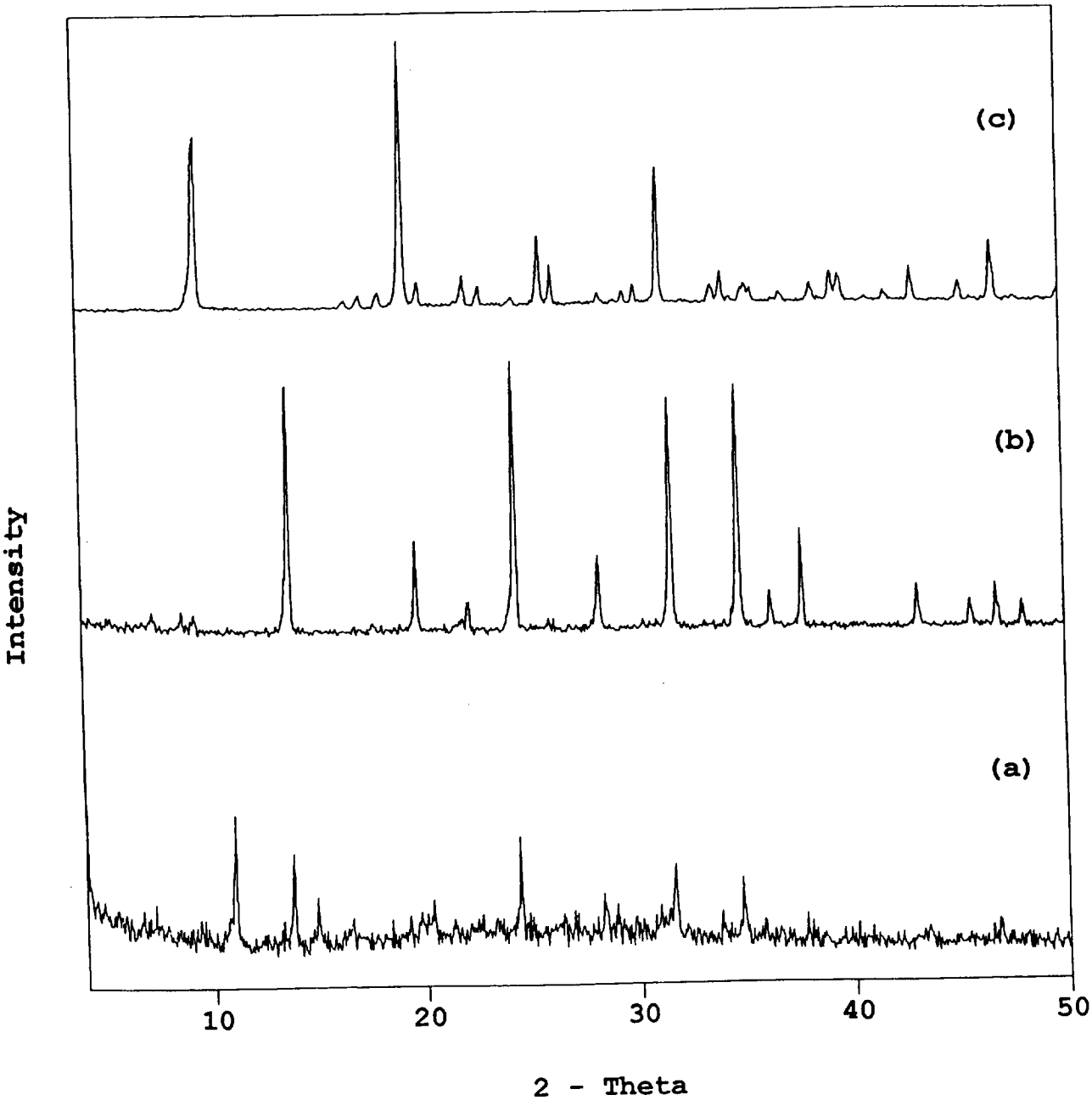
(c)
(b)
(a)
Intensity
10
20
30
40
50
2 - Theta

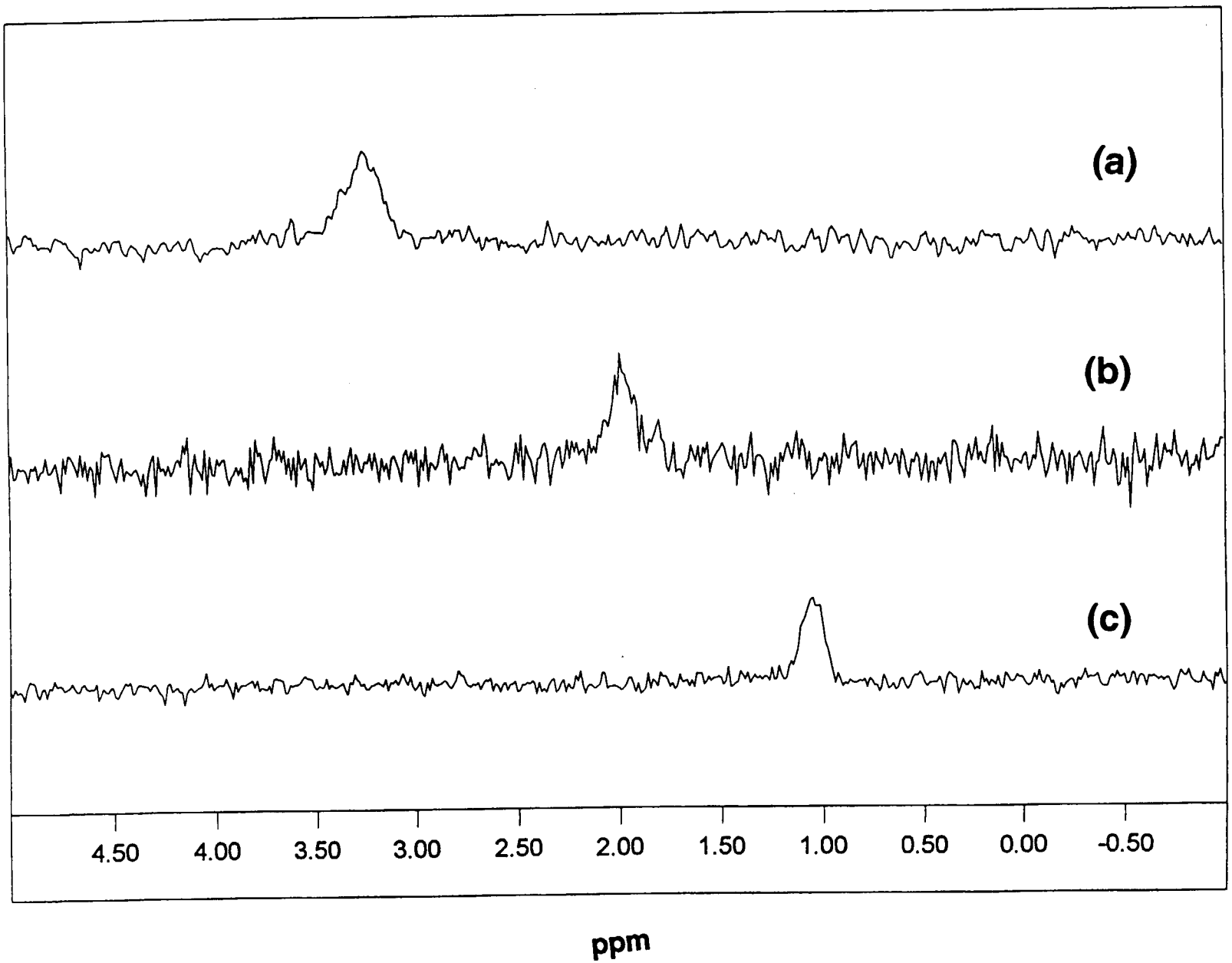
(a)
(b)
(c)
4.50
4.00
3.50
3.00
2.50
2.00
1.50
1.00
0.50
0.00
-0.50
ppm

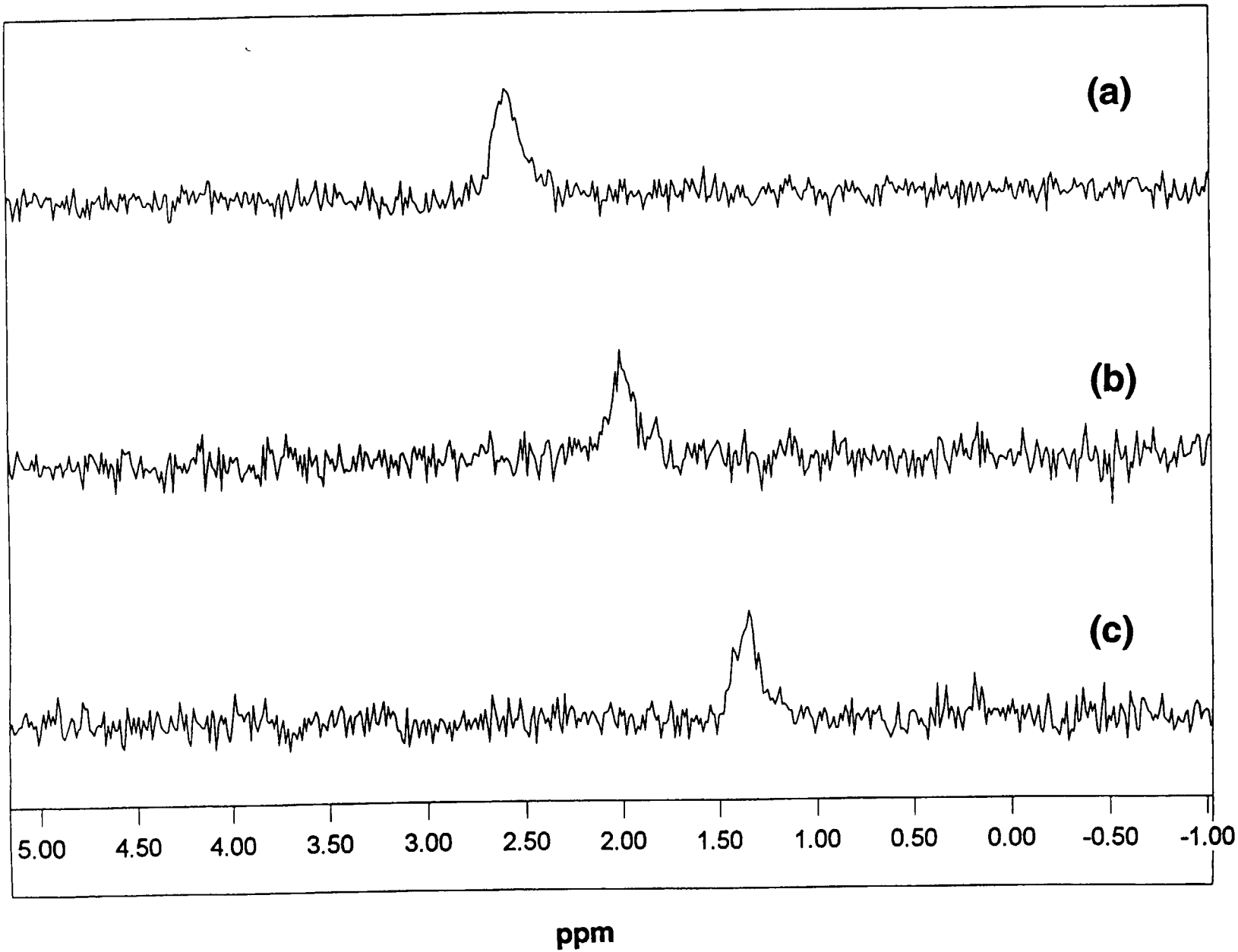

9

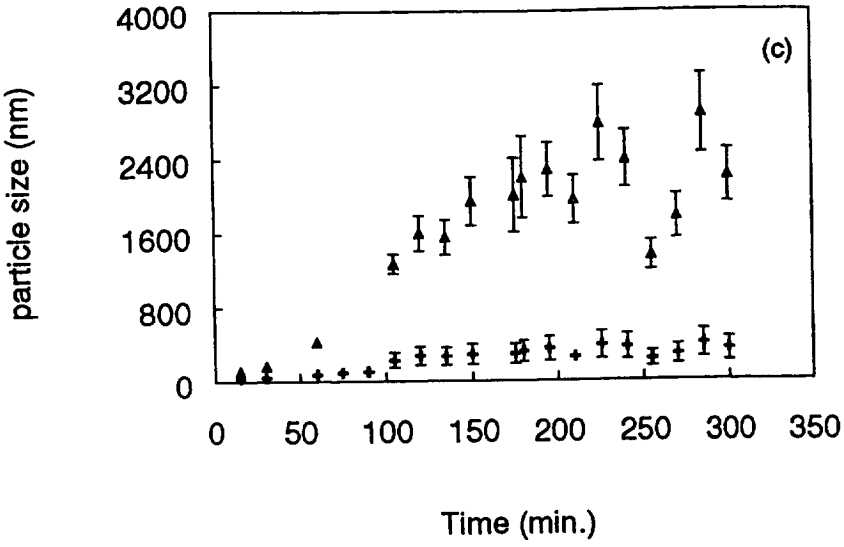
(c)
particle size (nm)
4000
3200
2400
1600
800
0
0
50
100
150
200
250
300
350
Time (min.)

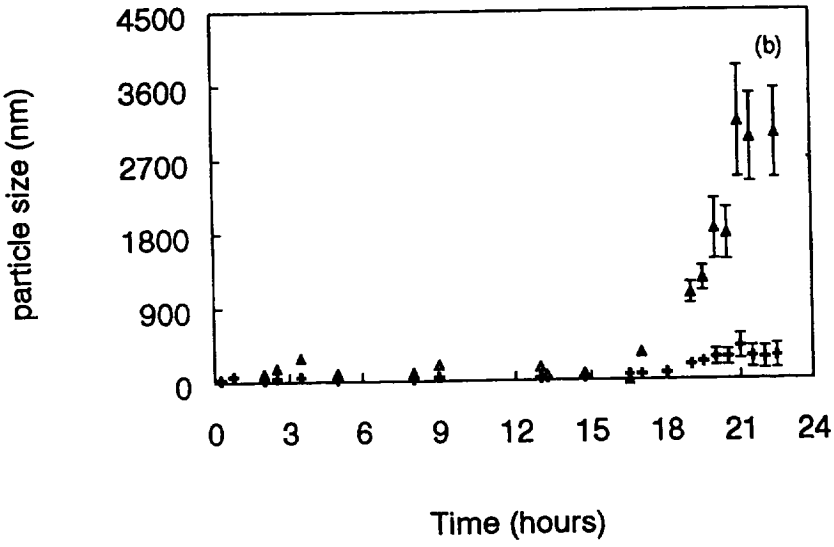
(b)
particle size (nm)
4500
3600
2700
1800
900
0
0
3
6
9
12
15
18
21
24
Time (hours)

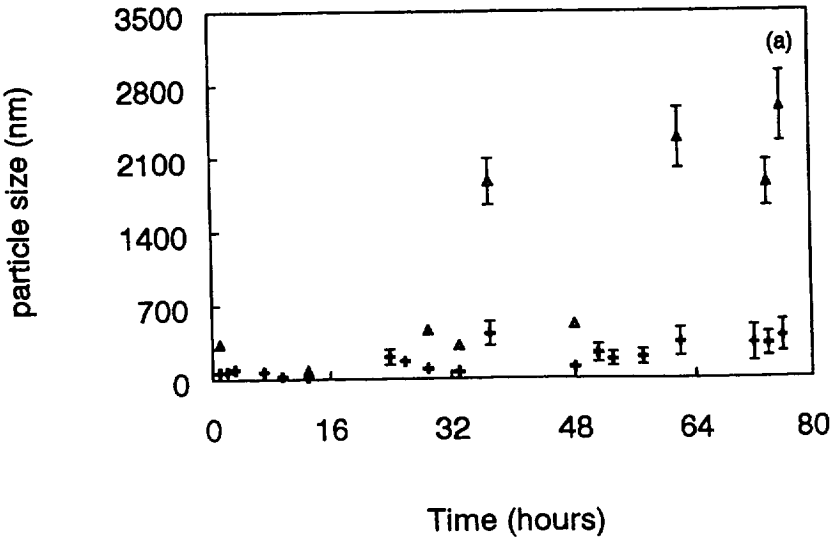
(a)
particle size (nm)
3500
2800
2100
1400
700
0
0
16
32
48
64
80
Time (hours)

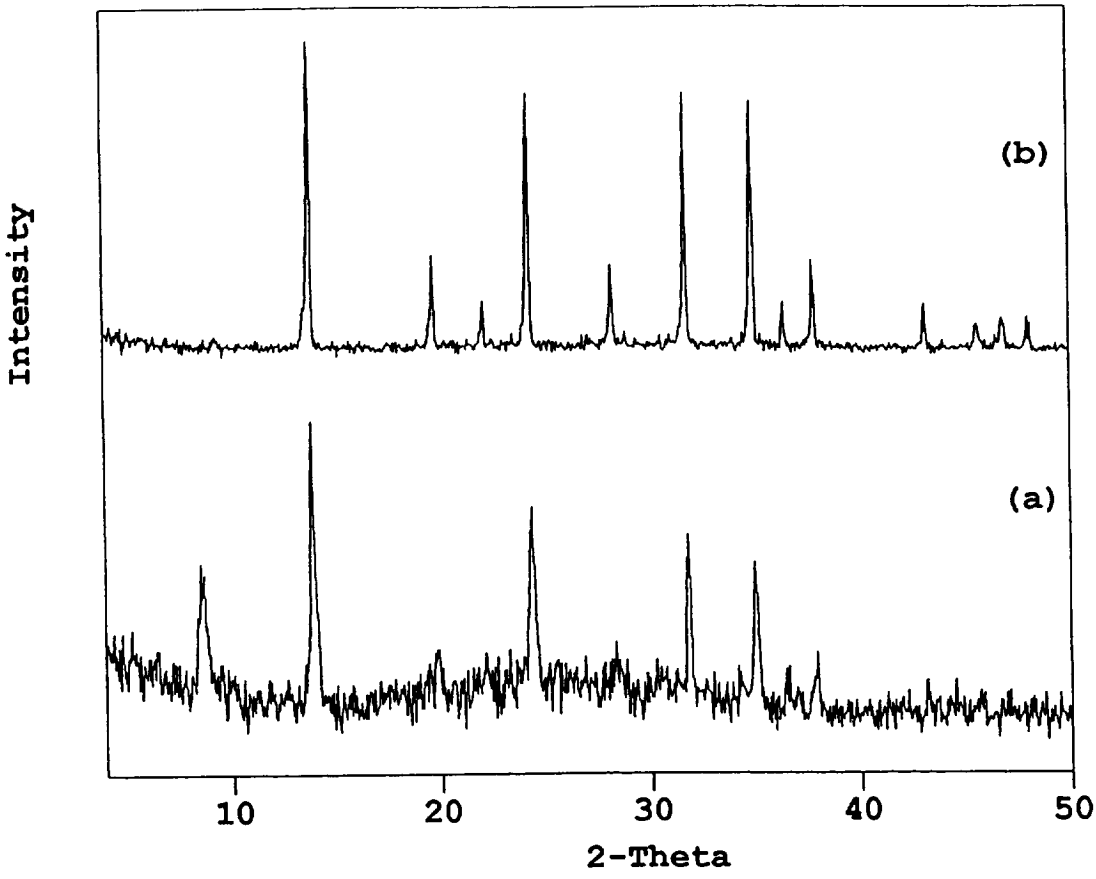
Intensity
(b)
(a)
10
20
30
40
50
2-Theta

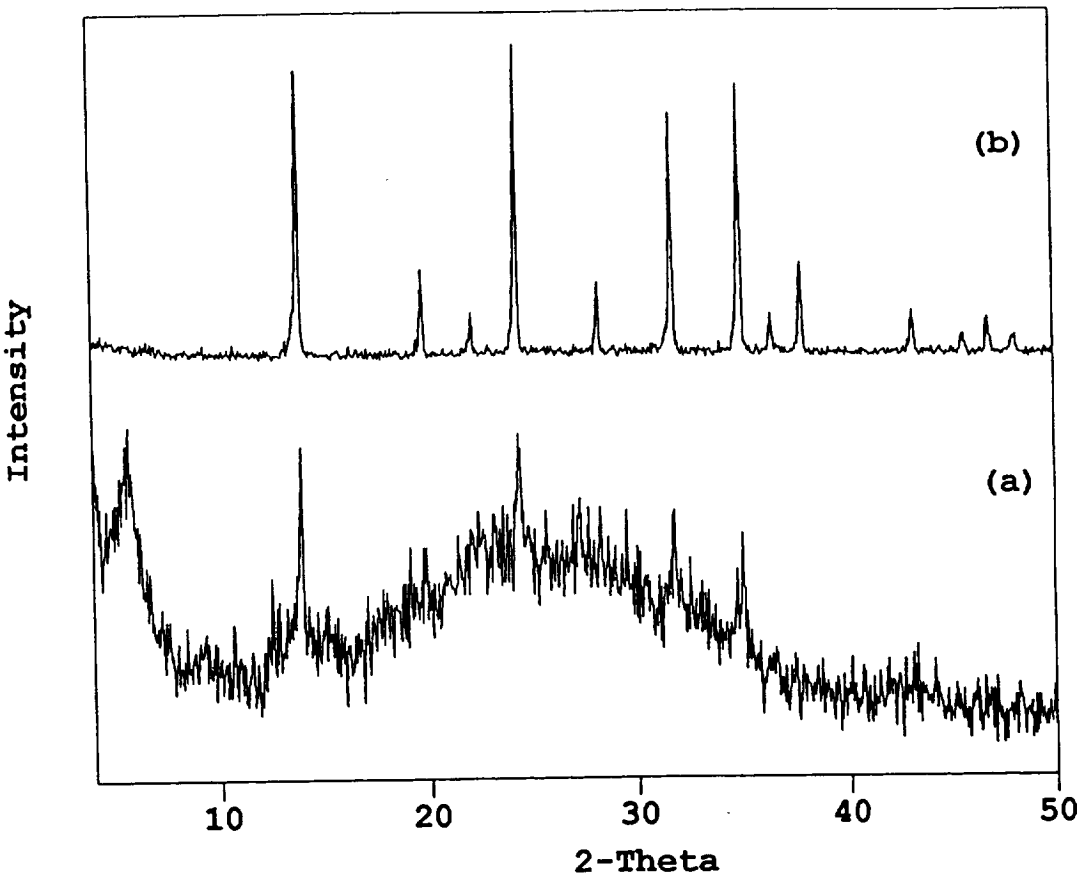
Intensity
(b)
(a)
10
20
30
40
50
2-Theta

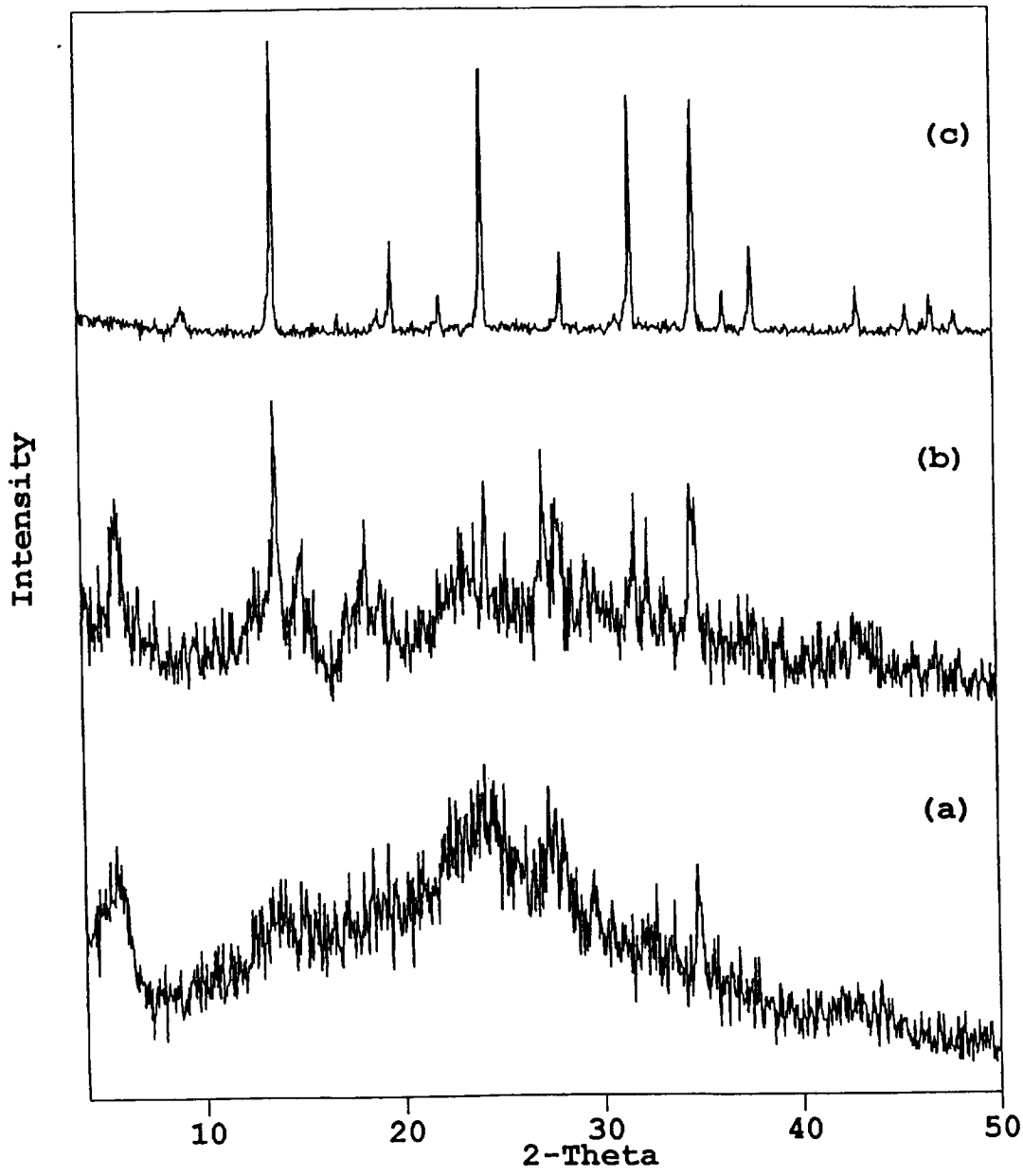
(c)
(b)
(a)
Intensity
10
20
30
40
50
2-Theta

(b)

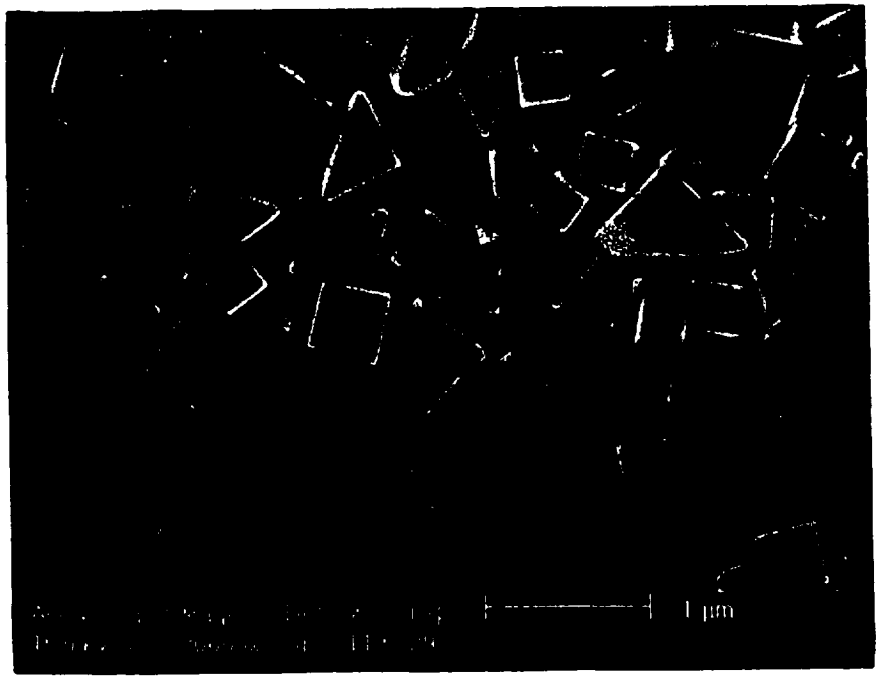

(a)

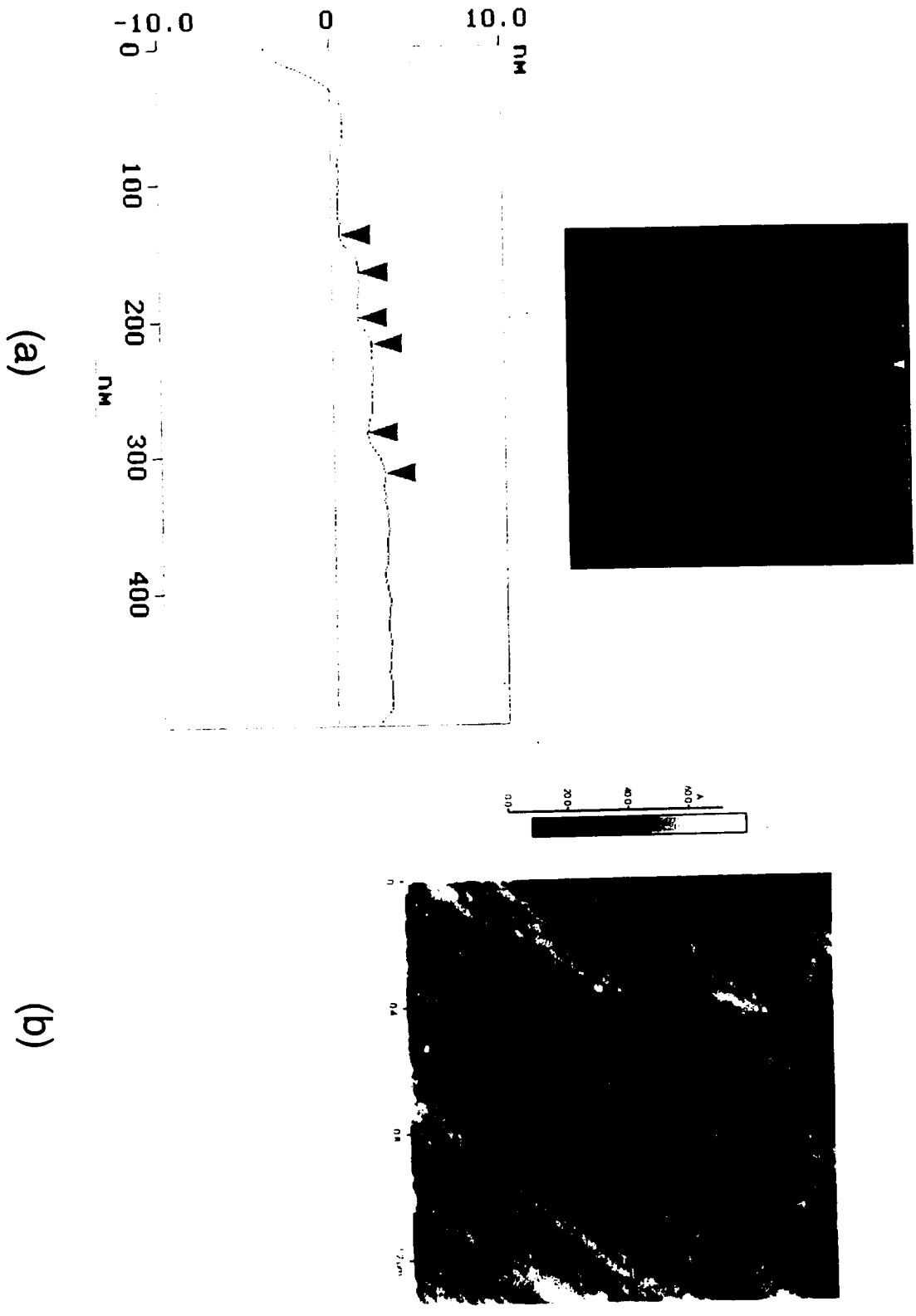
(a)
-10.0
0
10.0
nm
0
100
200
300
400
nm
(b)

(b)

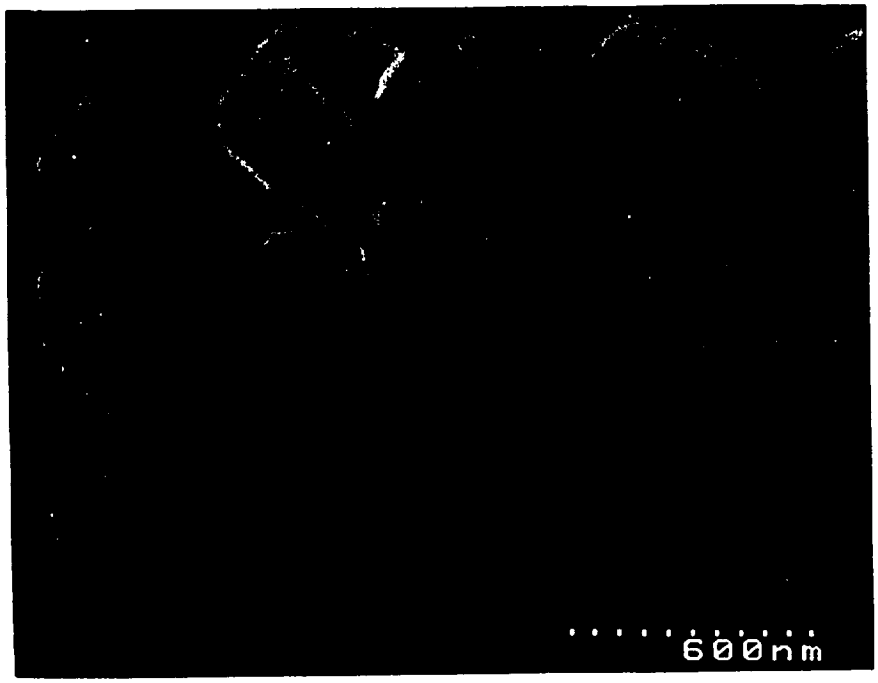

(a)

(c)

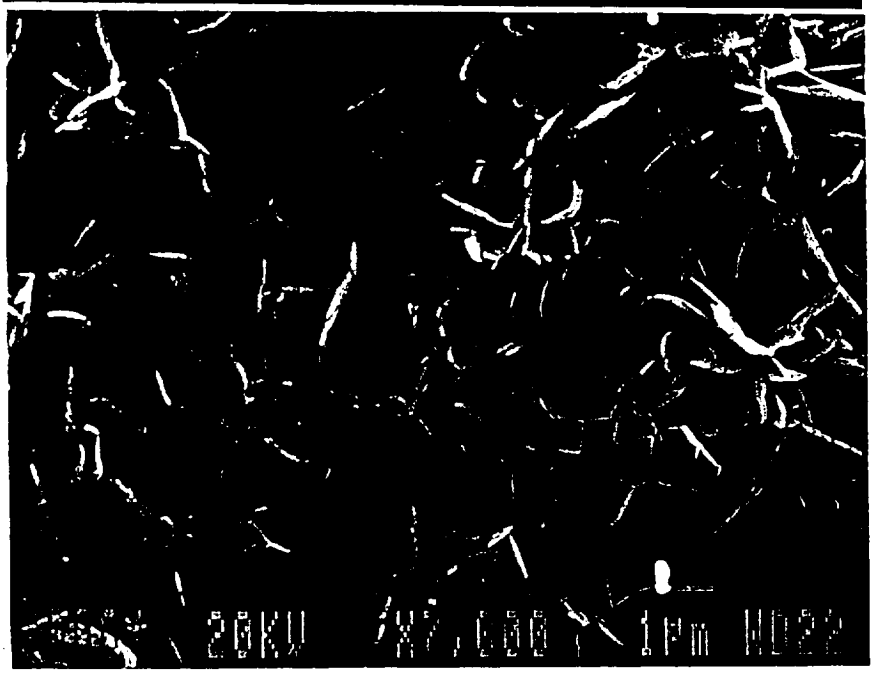
20KU X7,000 1Pm

(b)

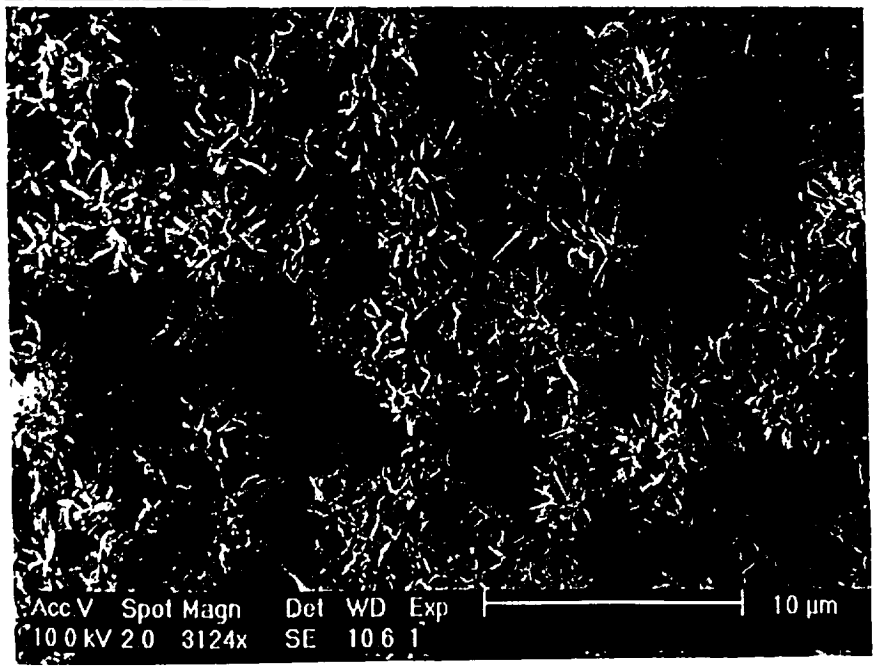
Acc.V Spot Magn Det WD Exp
10.0 kV 2.0 3124x SE 10.6 1
10 µm

(a)

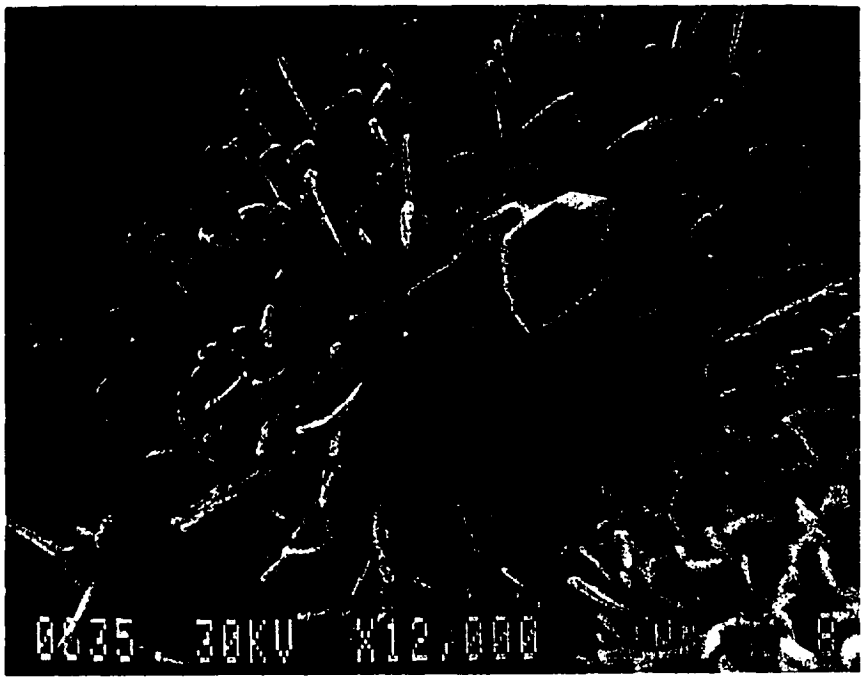

(b)

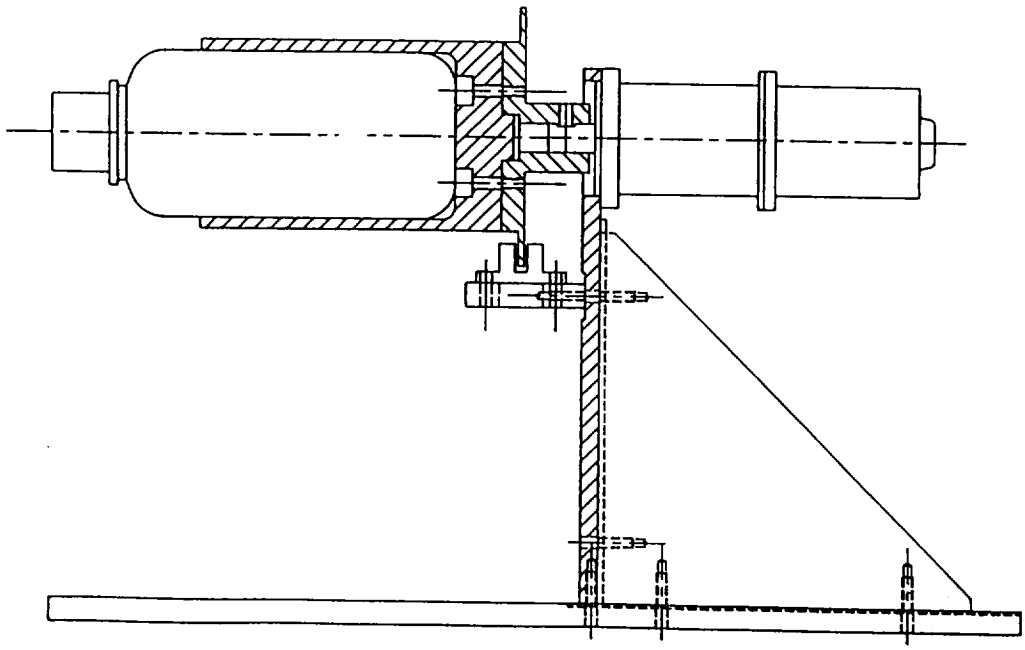

(a)